Development of High-sensitivity Photodetector Using Amorphous Selenium Photoconductor and Nitrogen-doped Diamond Cold Cathode

アモルファスセレンと窒素添加ダイヤモンド冷陰極を用いた高感度光検出器の開発

A Dissertation Presented to
The Graduate School of Arts and Science,
International Christian University,
For the Degree of Doctor of Philosophy

国際基督教大学　大学院
アーツ・サイエンス研究科提出博士論文

Masuzawa, Tomoaki
増 澤　智 昭

January 20th, 2014
２０１４年　１月２０日

Synopsis

Amorphous selenium (a-Se) is a promising material for a high-sensitivity photodetector that has low thermal noise and a wide detectable wavelength range that covers visible to the UV, as well as X-rays. The high sensitivity of a-Se based photodetector is explained by signal enhancement due to an internal carrier multiplication. The efficiency of the photon-signal conversion is higher than 1,000 % for a-Se based imaging tube called HARP [1], while the conversion efficiency is approximately 95 % for a standard silicon CCD. The unique carrier multiplication in a-Se should lead to ultra high-sensitivity imaging devices for the wavelengths covering visible to X-ray, although, the unknown physics of carrier multiplication has prevented further progress; as of now, a lucky-drift carrier multiplication mechanism has been proposed through empirical calculations and simulations [2].

In this dissertation, mechanism of high-sensitivity photo detection utilizing carrier multiplication in a-Se has been investigated. An a-Se based prototype photodetector has been developed in order to evaluate its sensitivity in multiplication mode. Nitrogen-doped diamond was used to drive this device, aiming that the advantages of diamond cold cathode such as high stability and low-energy electron contribute to the device operation.

As a result, the carrier multiplication and high-sensitivity photo detection have been confirmed, and the nominal quantum efficiency of a-Se based photodetector was estimated to be 10 to 40 for visible light and as large as 1,000 for UV light. The wavelength-dependence of the carrier multiplication process should help further clarify the mechanism of carrier multiplication, which should lead to high-sensitivity imaging in the wavelength beyond visible and UV.

[1] K. Tanioka, et al. IEEE Electron Device Letters, EDL-8, 9, 392-394 (1987)
[2] S. Kasap, et al. J. Appl. Phys. 96 2037 (2004)

Acknowledgement

First and foremost, I would like to thank my family and friends, who have been invaluable in supporting me through 4 years of PhD course, including the days of depression and a half the year of illness.

I would like to express my deepest gratitude to my supervisor, Professor Ken Okano, for his continuous support and great patience to supervise such a hardheaded student.

I am thankful to Dr. Takatoshi Yamada, who has been supporting me through these years, with a great patience and kindness.

I am thankful to the following people who I worked with, for their invaluable support and inspiring discussions:
Professor Yuji Takakuwa and Shuichi Ogawa at Tohoku University.
Professor Daniel Chua and Dr. Angel Koh at National University of Singapore.
Professor Hidenori Mimura and Professor Yoichiro Neo at Shizuoka University.
Dr. Tomonori Nakamura at Onizuka Glass Co.

Table of contents

Chapter 1. Introduction

1.1. Motivation

For centuries, scientists and engineers have attempted to replicate human vision and developed state-of-art devices such as complementary metal oxide semiconductor (CMOS) and charge-coupled devices (CCD). High-gain Avalanche Rushing amorphous Photoconductor (HARP) was one of the first successful photo imagers to exceed the sensitivity of a human eye [1], however, during its development, researchers found that a-Se possesses sensitivity beyond the visible light region; such as X-rays where a-Se X-ray imaging devices were proposed [2]. In addition, detection of weak ultraviolet (UV) light has attracted much attention in various fields, including astronomic observation, flame sensors for security use, transparent photovoltaic devices, as well as medical imaging [3-6]. A common UV detector is the avalanche photodiode (APD) made from silicon, however, this device has high thermal noise due to a relatively narrow band gap. While using wide-gap semiconductors can reduce the thermal noise, APDs made from wide-gap semiconductors are not sensitive to visible light, and are not suitable for spectrometric applications.

Amorphous selenium (a-Se) is a promising material for a high-sensitivity photodetector that has low thermal noise and a wide detectable wavelength range that covers visible to the UV [7], as well as X-rays [8-10]. The high sensitivity of a-Se based photodetector is explained by signal enhancement due to an internal carrier multiplication. Like other photoconductive materials, amorphous selenium generates electron hole pairs

when it is exposed to light. This means that the current that flows through the material increases when it is illuminated. What is unique in a-Se is that the photo-generated carriers are multiplied while drifting in the a-Se film, which enhances the electric signal and enables high-sensitivity photo detection. The efficiency of the photon-signal conversion is higher than 1,000 % for a-Se based imaging tube called HARP [1], while the conversion efficiency is approximately 95 % for a standard silicon CCD. The unique carrier multiplication in a-Se should lead to ultra high-sensitivity imaging devices, although, the unknown physics of carrier multiplication has prevented further progress; as of now, a lucky-drift carrier multiplication mechanism has been proposed through empirical calculations and simulations [11,12].

In the present study, the mechanism and conditions of carrier multiplication is being investigated in order to utilize this phenomenon in the wavelength range beyond visible light. To simplify the problem, we focus on a single-cell photodetector rather than imaging device, and attempt to fabricate a high-sensitivity photodetector. As a result, a prototype multi-wavelength photodetector has been assembled and high-sensitivity photodetection has been demonstrated utilizing carrier multiplication.

1.2. Current issues in a-Se based photodetectors and photo imagers

a-Se is one of the earliest materials in the history of amorphous semiconductors, and photoelectric interaction in selenium is known as early as mid 1900s. The resistivity of a-Se was drastically reduced by light illumination, which enables one to convert light into electronic signal. This photo-induced change of resistivity was named photoconductivity, and such element was called photoconductor. In 1948, Schaffert and Oughton developed the first xerography by using selenium thin-film as photoconductor [13]. The photoconductivity of a-Se was then used for imaging devices, which gave birth to camera

device called vidicon tubes. A vidicon tube is a vacuum device that consists of a photoconductive target and an electron source that enables it to scan and read out from the target.

A vidicon target called SATICON was developed by Hitachi, which was the first vidicon target using a-Se. Joined by the Japanese Broadcasting Corporation (NHK) research and development team, this target was further improved, and High-gain Avalanche Rushing amorphous Photoconductor (HARP) was invented in the 1980s. The significance of HARP target was that it could enhance the signal gain by utilizing impact ionization of the accelerated electrons and holes generated in the target film, as illustrated in Figure 1.2.1. This signal enhancement effect, named as *avalanche multiplication*, enables one to take a clear picture at extremely low illuminance. Although a-Se is not used for mainstream household devices, it has been utilized for high definition imaging technology.

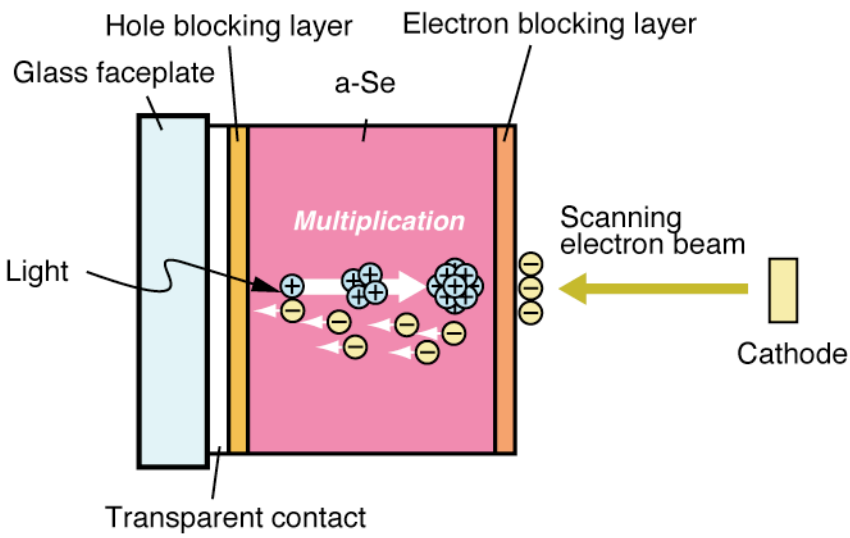

Figure 1.2.1. Schematic diagram explaining carrier multiplication [14].

One of few drawbacks of the HARP camera tube was that it required a hot cathode for signal read-out, which led to high power consumption and limited lifetime, as well as restriction in downsizing due to the electron scanning mechanism. A typical HARP camera tube was 10 cm in length, which prevents the device to be competitive to commercially available silicon-based imaging devices. Recently, much smaller versions of HARP camera tube have been developed by using field emitter arrays (FEAs). In FEA-HARP, hot cathode used as signal read-out was replaced with field emitter, as depicted in Figure 1.2.2. The field emitter is a device, where electron beam is obtained under intense electric field: the electrons are emitted through quantum tunneling effect, not by thermal excitation. Since the field emitter does not require high temperature to operate, it is often referred as cold cathode. By using arrayed field emitters, scanning of electron beam is not necessary, which can greatly reduce the size of the device.

Although FEA-HARP can greatly reduce the device size and promising as future imaging device, the use of FEA-HARP has been limited in visible-light imaging, with a few exception in soft X-ray [15,16]. The reasons to this are stability of selenium target, as well as some randomness in carrier multiplication. These factors seem to originate in lack of material characterization and suggest a need in further optimization of a-Se film for multi-wavelength application.

Another issue in current FEA-HARP arises due to the growing demand for high-definition (high-resolution) imaging technology. Although HARP camera tube is capable of taking full Hih-Vision image (1080i: 1920×1080 pixels), better resolution is required for the upcoming high-definition televisions such as 4K2K (4,000 x 2,000 pixels). To achieve such a high resolution, the field emitter for the signal read-out needs to be re-defined, since it restricts the resolution of the FEA-HARP. The field emitters used in

current FEA-HARP suffer from resolution loss caused by point-charge like electric field. Since field emission requires intense electric field of a few thousand volts per micrometer, typical field emitters have sharp tips on its surface to utilize geometrical field enhancement. Although these tips can greatly reduce the operation voltage of the emitter, it results in point-charge like potential distribution, and thus leads to dispersion of emitted electron beam [17-19]. As such, current FEA-HARP requires special treatment for electron convergence, either by introducing bulky magnet or fabricating multi-gated field emitters, both of which makes the device structure further complicated and increase its fabrication cost. In order to achieve the high spatial resolution, redesign of field emitter is mandatory.

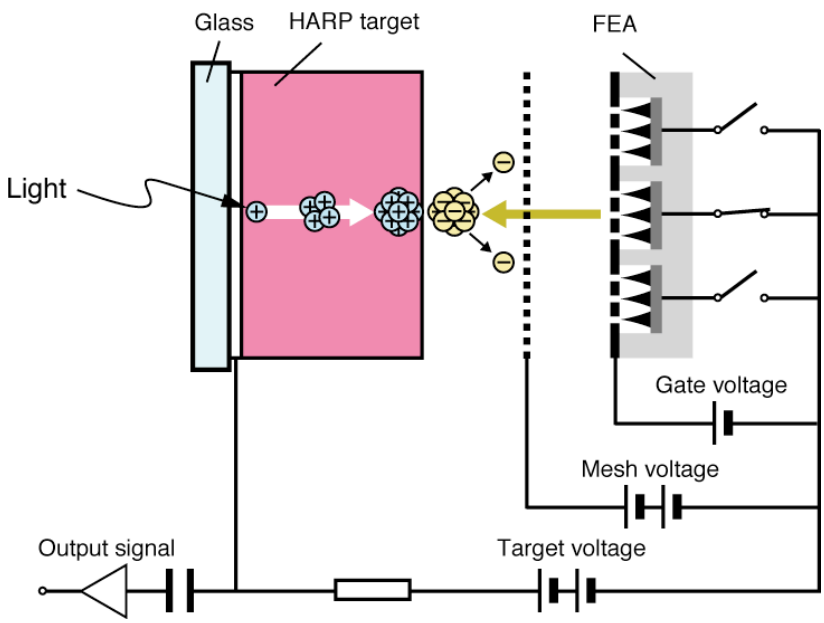

Figure 1.2.2. Schematic device structure of FEA-HARP [28].

An alternative application was suggested for a-Se. X-ray photoconductivity was discovered in the 1940s and opened up a realm of xeroradiography, or electrical collection of X-ray image. An advantage of a-Se in wide-area deposition was suitable to be combined with thin film transistor technology, whose collaboration resulted in new range of

flat-panel X-ray detector [8-10]. Figure 1.2.3 illustrates a structure of a-Se based flat-panel detector proposed by Kasap *et al*. The a-Se based flat-panel detector (FPD) has found its application in medical diagnosis, however, this type of X-ray detector has relatively high noise due to limited insulation, and its operation in high-sensitivity mode utilizing carrier multiplication has been limited due to uncontrolled breakdown in a-Se film and FET for signal read-out.

The cause of this breakdown is a local field enhancement in the device. Since the high-sensitivity mode requires electric field of 80–100 V/μm across the a-Se film [1], the operation voltage of a-Se FPDs is typically 1–1.5 kV. Such a high voltage often leads to breakdown of FET gate [20], as well as irreversible breakdown of a-Se layer due to a local field enhancement at the edge of metal electrode [21,22]. The local electric field can be reduced by introducing resistive interface layer, however, it sacrifices carrier transport property. Bubon et al. recently optimized the resistive interface layer, and reported a multiplication gain of 200 while maintaining the carrier transport properties [22]. An alternative approach was to fabricate a hole-blocking layer, which prevents hole injection from back contact and help applying a high voltage across a-Se film [23].

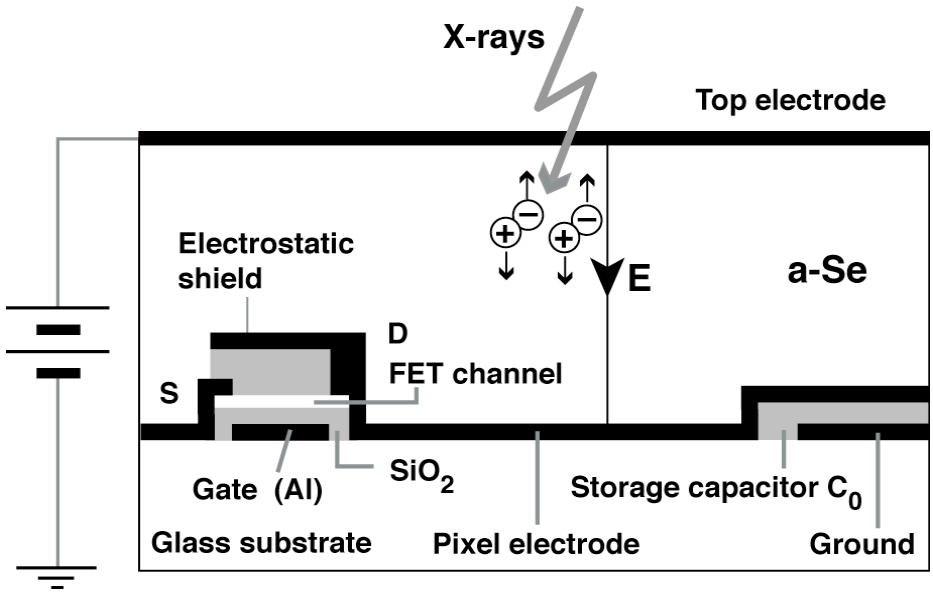

Figure 1.2.3. Schematic device structure of X-ray FPD [22].

Although these technologies seem to be promising for a-Se layers with limited thickness (~a few tens of microns), better insulation techniques are needed for chest radiography and computed tomography: in such applications, X-ray of up to 100 keV is utilized, which is so permeable that it requires a-Se layer ten times thicker than typical HARP films (a few hundred microns ~ 1 mm) to maintain its sensitivity. In that case, vacuum-tube type devices are necessary for their advantage of vacuum insulation.

Another remaining problem in a-Se based high-sensitivity X-ray detector is signal fluctuation due to the photo capturing process. Since the X-ray photons are much more energetic than those of visible light, the photons penetrate into a-Se photoconductor before interacting with it: since the penetration depth is limited by attenuation depth and is statistically distributed, this variation leads to signal fluctuation and may degrade image quality [24,25]. This signal fluctuation is an elemental issue that must be overcome for detecting high-energy X-ray. A possible solution is adding impurity atoms with large capture cross-section, such as Te or Pb.

To summarize the section, following issues need to be solved in order to achieve high-sensitivity a-Se based photodetector for wavelengths covering visible to X-ray:

a) Optimize a-Se target to increase its structural stability and induce carrier multiplication for multi-wavelength photo detection.
b) Re-design the signal read-out for better spatial resolution and maximum carrier multiplication gain.
c) Establish the way to control photo absorption and carrier multiplication in high photon energy region. Especially, the depth, where X-ray photons are captured in a-Se, needs to be controlled.

Issue a) and c) are closely related to the material characterization of a-Se, as well as mechanism of carrier multiplication. Issue b) seems to be less important in a single-cell photodetector without imaging capability, however, it has been found that optimization of the cathode is also important in photodetector, since a-Se target can degrade by electron beam irradiation.

In order to solve these issues, a novel device needs to be developed, with a-Se target optimized for multi-wavelength photo detection and cold cathode for high resolution and effective signal read-out. Toward this goal, optimization of both a-Se target and cold cathode is being investigated. Optimization of a-Se film has been conducted to solve issue a), and it has been found that stabilization of a-Se film is a key factor to achieve high-sensitivity mode utilizing carrier multiplication. In addition, issue b) was examined by using nitrogen(N)-doped diamond as cold cathode. As described in the next section, the use of N-doped diamond can contribute to both high-sensitivity operation and high-resolution when used in imaging device. Issue c) is listed as a future task: in addition to the stabilization of a-Se, there should be issues specific to X-ray detection, as mentioned above.

1.3. N-doped diamond as a cold cathode

As mentioned in the previous section, vacuum tube device is advantageous over solid-state photodetector for its vacuum insulation and low dark current. In order to develop a novel device for high-sensitivity photo detection in visible to X-ray region, diamond cold cathode can be a promising choice to solve the current problems of FEA-HARP.

Field-induced electron emission, or simply field emission, is a phenomenon

where electrons are emitted from a surface of material under existence of intense electric field. Unlike thermionic emission and photoemission, electrons are emitted into vacuum due to the quantum tunneling effect. To describe this, one can assume that electrons are trapped in a material due to a potential barrier at the material surface. The shape of the potential barrier is modified by external electric field. When the external electric field is intense enough, the potential barrier becomes thin enough to allow electrons in the material to tunnel through it and emitted into vacuum [26].

Since the field emission process involves in electron tunneling through the potential barrier, materials having small potential barrier is preferable for field emitter application. Diamond is famous for its hydrogen-terminated surface having negative electron affinity (NEA). The negative electron affinity suggests that the potential barrier between the conduction band and the vacuum level is negative: in other words, if diamond has electrons in the conduction band, these electrons can be emitted into vacuum without extra energy. For this reason, diamond has been regarded as a promising material for cold cathode with low operation voltage and potential high current density.

However, due to the lack of shallow donor, diamond can hardly have electrons in its conduction band. This has prevented a development of practical NEA emitter. Heavily N-doped diamond is one of few examples that emit electrons utilizing negative electron affinity. Other examples are diamond p-n junction cathode and triple junction cathode, as well as n-type boron nitride.

The electron emission mechanism of the high resistive N-doped diamond cathode was summarized as follows using metal-insulator-vacuum (M-I-V) model [27]. Since heavily N-doped diamond has extremely high resistivity (>100 GΩcm) and is treated as an insulator, a strong electric field appears across the diamond film when bias is applied. This electric field induces electron tunneling from the back contact to the conduction band

of the diamond, and electrons are supplied in the diamond conduction band. The negative/zero electron affinity of diamond allowed the exponential increase in electrons injected into the diamond from the back contact to be reflected in an exponential rise in the field emission current. Figure 1.3.1 illustrates the schematic diagram explaining M-I-V type electron emission. This process gave rise to the extremely low threshold field electron emission (~ 0.5 V/μm) from the high resistivity N-doped diamond.

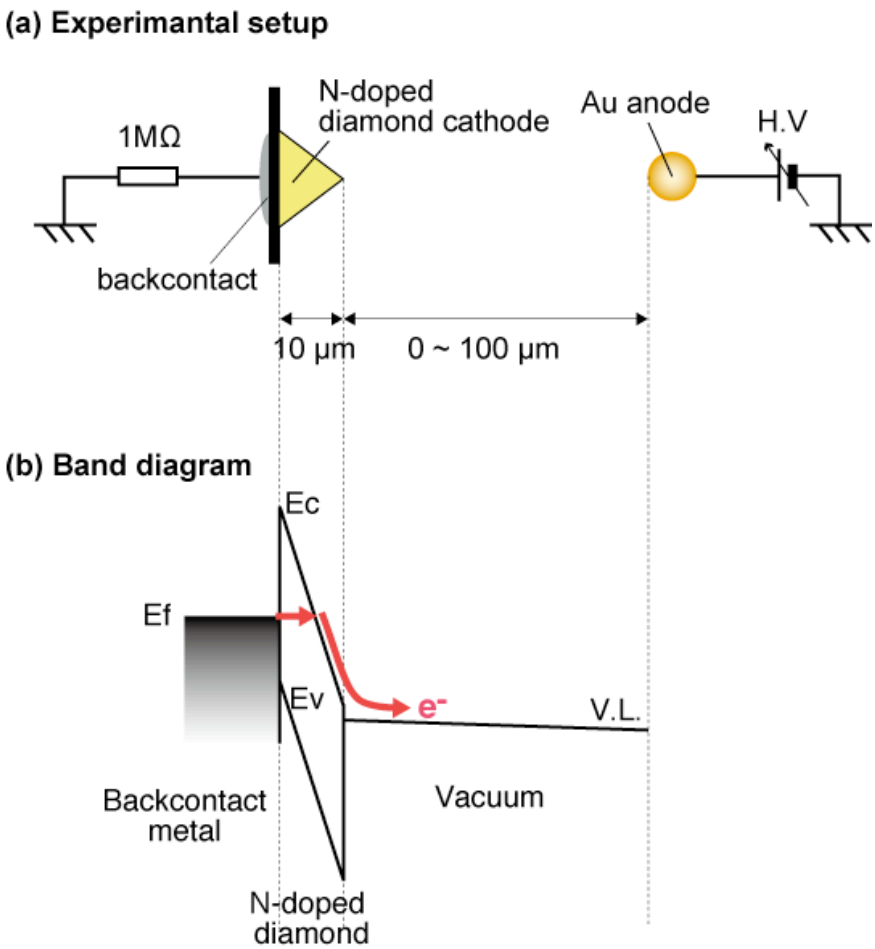

Figure 1.3.1. Schematic diagram of Metal-Insulator-Vacuum (M-I-V) type emission [27]: (**a**) experimental setup, (**b**) band diagram, where electron injection into diamond and electron emission from NEA are schematically drawn.

Looking back in the previous section, the current issue in a-Se based photodetector originated in the cathode was dispersion of electron beam. The electrons are dispersed by the point-like electric field, which is generated due to the sharp tips on the emitter surface. As M-I-V type emitter does not utilize field enhancement at the surface, electrons are emitted even from a flat surface. This contributes to smaller dispersion angle of emitted electrons and improves the spatial resolution of an imaging device. In addition, the M-I-V type emission can utilize negative electron affinity surface, which enables emission of low-energy electrons and can prevent the crystallization of a-Se. Finally, the emission stability of the cathode can greatly be increased, because hydrogenated surface of diamond is physically stable and durable against oxidization. The use of diamond cold cathode is, therefore, a promising choice for both high spatial resolution and high sensitivity utilizing carrier multiplication.

1.4. Previous studies on a-Se photodetector driven by diamond cold cathode

1.4.1. Diode structured photodetector

Amorphous selenium based photodetector using diamond cold cathode was first proposed by Suzuki et al. [28,29]. The a-Se anode and the diamond cathode were combined into a photodetector, whose structure is illustrated in Figure 1.4.1 [28]. The operational mechanism of this device was explained as follows: electron–hole pairs were generated in a-Se film by incident illumination through the glass faceplate. Those generated holes were accelerated toward the cathode side of a-Se film by the electric field between the anode and cathode. Surface potential of a-Se rose due to the presence of accumulated holes. Consequently, the extraction field/voltage of the diamond cathode increased, and more electrons were emitted from the cathode. When the illumination was turned off, the number of holes at a-Se surface decreased because less electron–hole pairs

were generated in the a-Se film. The extraction voltage of cathode, then, became lower and the emission current decreased. Thus, the illumination was detected as the modulation of the emission current from diamond cathode. Although this model could explain well the I-V characteristics of the photodetector, it was difficult to confirm it experimentally, since the surface potential of a-Se surface could not be measured due to the high resistivity of a-Se film. The proposed diode-type photodetector showed a stable operation even in a low vacuum around 10^{-5} Torr by virtue of diamond cold cathode, however the response time was relatively slow as shown in the Figure 1.4.2 [29].

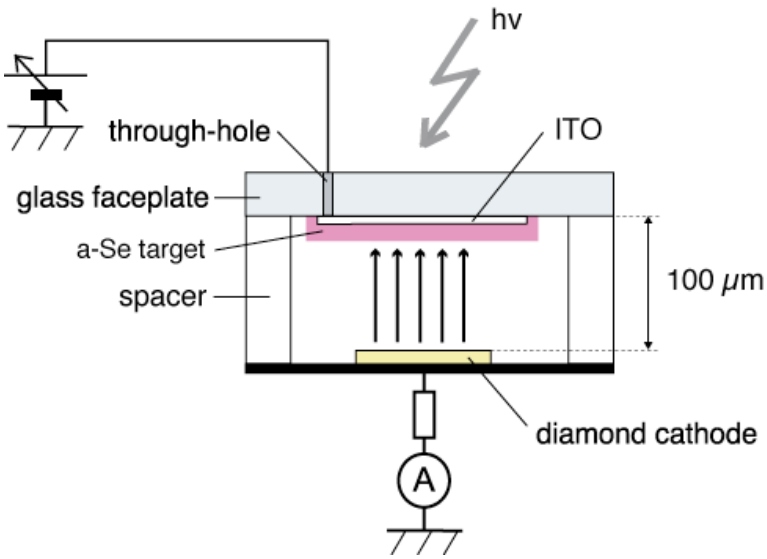

Figure 1.4.1. Schematic diagram of a diode-structured photodetector that consists of a-Se photoconductive anode and N-doped diamond cold cathode, after ref [29].

The cause of this slow response was due to transient surface potential of a-Se. As mentioned in the operational mechanism, the extraction field/voltage of diamond in this photodetector depended on surface potential at a-Se. When illumination was on, the number of holes that accumulated at a-Se surface was increased due to the photo-generated holes, and the electrical potential at a-Se surface increased. Subsequently, the rise in

surface potential enhanced the electron emission from diamond. Emitted electrons, then, compensated holes at the surface, decreasing its potential. This transient increase of potential at the surface caused the emission current to increase slowly. When compensation was balanced, the emission current reached an equilibrium state. No or less photo-generated carriers were expected in the a-Se bulk when illumination was turned off. Accordingly, the potential at the a-Se surface decreased due to decrease in the number of holes at the surface, thus, the emission current decreased until it reached equilibrium.

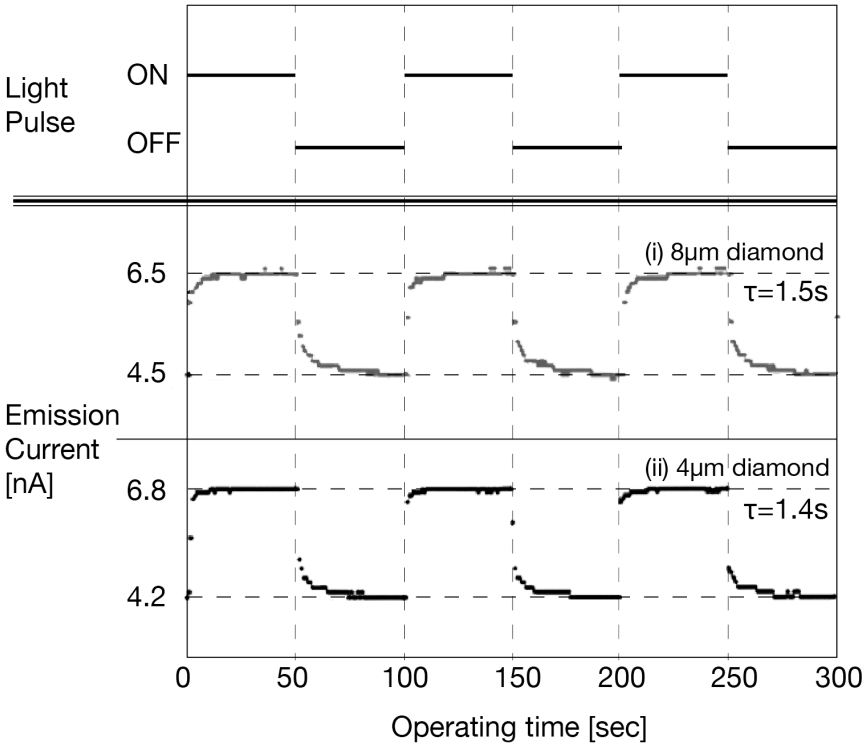

Figure 1.4.2. I-T characteristics of the diode-structured photodetector, which proved photo response. After Oonuki *et al.* in ref [29].

1.4.2. Triode structured photodetector and its time response

In order to improve the response time of the photodetector, triode-structured device was proposed by Suzuki *et al* [30]. By adding extraction grid above the cathode, as illustrated in Figure 1.4.3, this device enabled one to control electron supply from the cathode without transient change of surface potential of a-Se film.

The operational mechanism of the triode-structured photodetector was explained as follows. The back contact of the diamond film was electrically grounded and the extraction voltage was applied to the mesh grid to extract electrons from the diamond cathode. The emitted electrons were accelerated towards the grid and some of them could reach a-Se surface through the grid. At the same time, a positive voltage was applied to the anode. Photo-generation produced electron-hole pairs in the a-Se film when illuminated by light, and the holes were accelerated toward the cathode side of the a-Se surface. The accumulated holes at the a-Se surface gave rise to the number of electrons, which could reach the a-Se surface. The increase in electrons by incident illumination was detected as the increase in the anode current. The anode current depended not only on the illumination of the a-Se but also the anode voltage. When a higher anode voltage was applied, more holes were accelerated and accumulated at the a-Se surface. The anode voltage could continuously control the dynamic range of the anode current to the illumination.

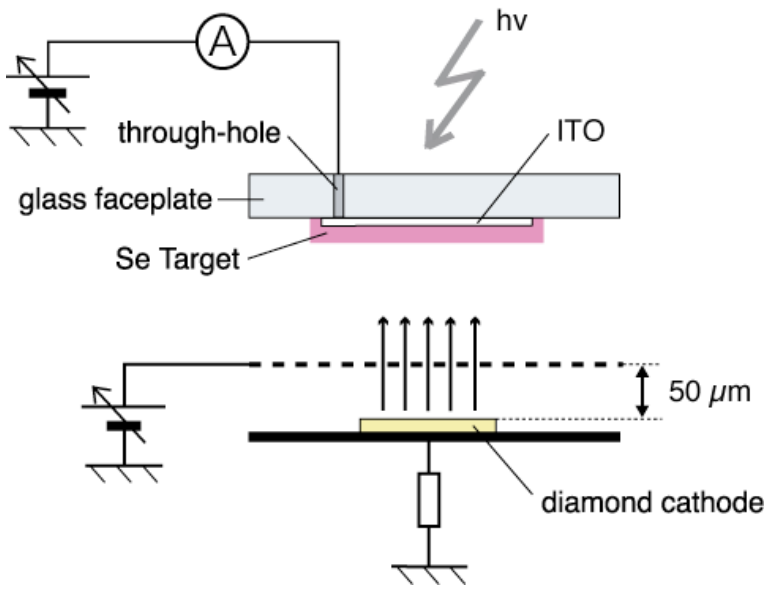

Figure 1.4.3. Schematic diagram of a triode-structured photodetector after Suzuki *et al* [30]. An extraction grid was introduced to control the emission current independent of a-Se surface potential.

As a result, the tails in the I-T chart was eliminated as shown in Figure 1.4.4(i-iii), which suggest that the response time of the triode structured photodetector has been improved. This result also indicated that the dynamic range of this photodetector could be controlled by the anode voltage. The next step is to apply high-sensitivity mode in these types of photodetector, utilizing carrier multiplication in a-Se.

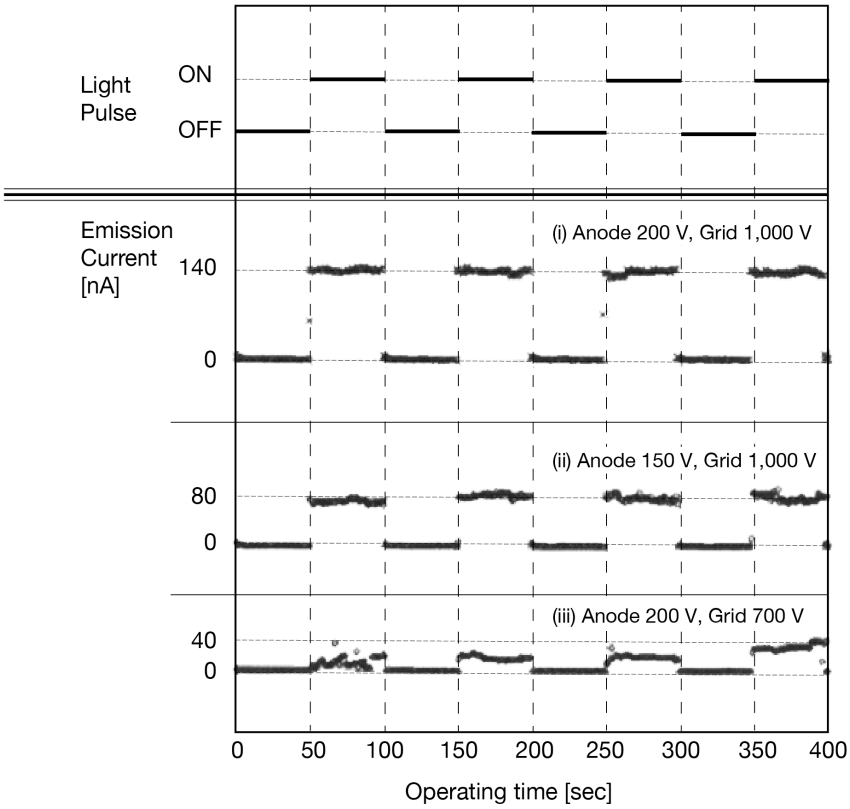

Figure 1.4.4. I-T characteristics of triode-structured photodetector after Suzuki *et al*. [30]. The bias conditions were (**i**) anode voltage 200 V and grid voltage 1,000 V, (**ii**) anode voltage 150 V and grid voltage 1000 V, (**iii**) anode voltage 200 V and grid voltage 700 V.

1.5. Scope of the dissertation

As mentioned in the previous section, a vidicon-type photodetector was proposed using a-Se target and diamond cold cathode. Using the diode and triode devices, a successful photodetection was confirmed, and low-vacuum operation at 10^{-5} Torr was reported. However, application of carrier multiplication for high-sensitivity photodetection has not been demonstrated. The next step is to apply high-sensitivity mode to these devices.

In this dissertation, an attempt has been made to investigate the mechanism of high-sensitivity photo detection utilizing carrier multiplication in a-Se. The elemental composition and the structure of a-Se films are characterized using time-of-flight secondary ion mass spectroscopy (TOF-SIMS) and Raman spectroscopy, so that the a-Se film is optimized for better stability to induce carrier multiplication. In addition, the a-Se film is combined with a N-doped diamond film to fabricate a prototype single-cell photodetector. Using this photodetector, operation mechanism of the high-sensitivity photo detection is investigated. As a result, a new operation mode is proposed, which enables high-sensitivity photo detection without having carrier-blocking layer at the surface of a-Se target. This new operation mode has allowed high-sensitivity photo detection, and the sensitivity has been evaluated in terms of external quantum efficiency. The high-sensitivity operation is then extended to the wavelength beyond visible light to the UV region, and demonstrated the sensitivity 1,000 times as high as latest UV sensors.

The fabrication and characterization of a-Se film is presented in Chapter 2, where phase-changing property of a-Se is investigated. In Chapter 3, diamond cold cathode is focused, in terms of nitrogen concentration and its field emission properties. Investigation of carrier multiplication in a-Se is focused in Chapter 4, where optimization of a-Se film is conducted for better stability and carrier multiplication. The optimized a-Se target is mounted on a prototype photodetector, and high-sensitivity photo detection has been demonstrated. The high-sensitivity mode is then extended to UV region, of which results are presented in Chapter 5.

References

[1] K. Tanioka, J. Yamazaki, K. Shidara, K. Taketoshi, T. Kawamura, S. Ishioka and Y. Takasaki, "An Avalanche-Mode Amorphous Selenium Photo- conductive Layer for Use as a Camera Tube Target," IEEE Electron Device Lett., EDL-8, 9, 392-394 (1987)

[2] S. O. Kasap and J. A. Rowlands, "X-ray photoconductors and stabilized a-Se for direct conversion digital flat-panel X-ray image- detectors," J. Mater. Sci., Mater. Electron. 11, 179-198 (2000)

[3] C H. Lin and C W. Liu, "Metal-Insulator-Semiconductor Photodetectors," Sensors 2010, 10, 8797- 8826 (2010)

[4] J. Yu, C X. Shan, Q. Qiao, X H. Xie, S P. Wang, Z Z. Zhang, and D Z. Shen, "Enhanced Responsivity of Photodetectors Realized via Impact Ionization," Sensors 2012, 12, 1280-1287 (2012)

[5] X. Gong, M H. Tong, S H. Park, M. Liu, A. Jen and A. J. Heeger, "Semiconducting Polymer Photodetectors with Electron and Hole Blocking Layers: High Detectivity in the Near-Infrared," Sensors 2010, 10, 6488-6496 (2010)

[6] I. Saito, W. Miyazaki, M. Onishi, Y. Kudo, T. Masuzawa, T. Yamada, A.T.T. Koh, D.H.C. Chua, K. Soga, M. Overend, M. Aono, G.A.J. Amaratunga, and K. Okano, "A transparent ultraviolet triggered amorphous selenium p-n junction," Appl. Phys. Lett. 98, 152102 (2011)

[7] S. Abbaszadeh, K.S. Karim, and V. Karanassios, "Measurement of UV from a Microplasma by a Microfabricated Amorphous Selenium Detector," IEEE Trans. Electron. 60, 880-883 (2013)

[8] S. O. Kasap and J. A. Rowlands, "X-ray photoconductors and stabilized a-Se for direct conversion digital flat-panel X-ray image- detectors," J. Mater. Sci., Mater. Electron. 11, 179-198 (2000)

[9] S. O. Kasap and J. A. Rowlands, "Direct-conversion flat-panel X-ray image detectors," IEEE Proc.- Cirtuits Devices Syst. 149, 85-96 (2002)

[10] S. O. Kasap, J. B. Frey, G. Belev, O. Tousignant, H. Mani, J. Greenspan, L. Laperriere, O. Bubon, A. Reznik, G. DeCrescenzo, K. S. Karim and J. A. Rowlands, "Amorphous and Polycrystalline Photoconductors for Direct Conversion Flat Panel X-Ray Image Sensors," Sensors 2011, 11, 5112-5157 (2011)

[11] S. Kasap, J. A. Rowlands, S. D. Baranovskii and K. Tanioka, "Lucky drift impact ionization in amorphous semiconductors," J. Appl. Phys. 96 2037 (2004)

[12] A. Reznik, S. D. Baranovskii, O. Rubel, G. Juska, S. O. Kasap, Y. Ohkawa, K. Tanioka and J. A. Rowlands, "Avalanche multiplication phenomenon in amorphous semiconductors: Amorphous selenium versus hydrogenated amorphous silicon," J. Appl. Phys. 102, 053711 (2007)

[13] R. M. Schaffert and C. D. Oughton, "Xerography: A New Principle of Photography and Graphic Reproduction," J. Opt. Soc. Am.38, p991-998 (1948)

[14] K. Tanioka, J. Yamazaki, K. Shidara, K. Taketoshi, T. Kawamura, T. Hirai, Y. Takasaki and T. Unnai, "Avalanche-mode a-Se Photoconductive Target for High Sensitive Camera Tube," Journal of the Institute of Image Information and Television Engineers 44, No. 8, pp.1074-1083 (1990)

[15] T. Miyoshi, N. Igarashi, N. Matsugaki, Y. Yamada, K. Hirano, K. Hyodo, K. Tanioka, N. Egami, M. Namba, M. Kubota, T. Kawai and S. Wakatsuki, "Development of an X-ray HARP–FEA detector system for high-throughput protein crystallography," J. Synchrotron Rad. 15, 281–284 (2008)

[16] Y Ohkawa, "Improving the picture quality of ultra-high-sensitivity HARP imaging devices,", NHK R and D/No.122/2010.7

[17] Y. Takiguchi, M. Nanba, K. Osada, T. Watabe, S. Okazaki, N. Egami, K. Tanioka, M. Tanaka, and S. Itoh, "256×192 pixel field emitter array image sensor with high-gain avalanche rushing amorphous photoconductor target," J. Vac. Sci. Technol. B 22, 1390 (2004)

[18] N. Egami, M. Nanba, Y. Takiguchi, K. Miyakawa, T. Watabe, S. Okazaki, K. Osada, Y. Obara, M. Tanaka, and S. Itoh, "50×50 μm pixel magnetic focus field emitter array image sensor with high- gain avalanche rushing amorphous photoconductor target," J. Vac. Sci. Technol. B 23, 2056 (2005)

[19] T. Nakada, T. Sato, Y. Matsuba, K. Sakemura, Y. Okuda, N. Negishi, A. Watanabe, T. Yoshikawa, K. Ogasawara, M. Nanba, K Tanioka, N. Egami, A. Kobayashi, and N. Koshida, "2/3 in. ultrahigh-sensitivity image sensor with active-matrix high-efficiency electron emission device," J. Vac. Sci. Technol. B 28, C2D11 (2010)

[20] M. Nakayama, H. Ohtake, M. Yamauchi, T. Tajima, T. Watabe, Y. Takiguchi, Y. Ishiguro, T. Hayashida, T. Watanabe and M. Abe, "A High-voltage MOSFET Applicable to a Highly Sensitive Solid-state Imager," Journal of the Institute of Image Information and Television Engineers, Vol. 53, No. 1, 142-147 (1999)

[21] M. M. Wronski, W. Zhao, A. Reznik, K. Tanioka, G. DeCrescenzo, and J. A. Rowlands, "A solid- state amorphous selenium avalanche technology for low photon flux imaging applications," Med. Phys. 37 (9), 4982-4985 (2010)

[22] O. Bubon, G. DeCrescenzo, W. Zhao, Y. Ohkawa, K. Miyakawa, T. Matsubara, K. Kikuchi, K. Tanioka, M. Kubota, J.A. Rowlands and A. Reznik, "Electroded avalanche amorphous selenium (a-Se) photosensor," Curr. Appl. Phys. 12 983 (2012)

[23] S. Abbaszadeh, N. Allec, S. Ghanbarzadeh, U. Shafique and K.S. Karim, "Investigation of Hole- Blocking Contacts for High-Conversion-Gain Amorphous Selenium Detectors for X-Ray Imaging," IEEE Trans. Electron Devices 59, no.9, pp.2403-2409 (2012)

[24] G. Hajdok, J. Yao, J. J. Battista and I. A. Cunningham, "Signal and noise transfer properties of photoelectric interactions in diagnostic x-ray imaging detectors," Med. Phys. 33, (10) 3601-3620 (2006)

[25] B. J.M. Lui, D. C. Hunt, A. Reznik, K. Tanioka and J. A. Rowlands, "X-ray imaging with amorphous selenium: Pulse height measurements of avalanche gain fluctuations," Med. Phys. 33, 3183 (2006)

[26] R. Gomer, "Field Emission and Field Ionization," Harvard U.P., Cambridge, Mass. (1961)

[27] K Okano, T. Yamada, A. Sawabe, S. Koizumi, J. Itoh, and G. A. J. Amaratunga, "Metal-insulator- vacuum type electron emission from N-containing chemical vapor deposited diamond," Appl. Phys. Lett. 79, 275-277 (2001)

[28] Y. Suzuki, H. Yamaguchi, K. Oonuki, Y. Okamura, and K. Okano, "Amorphous Selenium Photodetector Driven by Diamond Cold Cathode," IEEE Electron Device Lett. 24, 16-18 (2003)

[29] K. Oonuki, Y. Suzuki, H. Yamaguchi, K. Okano, and Y. Okamura, "Diode structure amorphous selenium photodetector with nitrogen (N)-doped diamond cold cathode," J. Vac. Sci. Technol. B 21, 1586 (2003)

[30] Y. Suzuki, K. Oonuki, H. Yamaguchi, Y. Okamura, and K. Okano, "Triode-structure amorphous selenium photodetector driven by diamond cold cathode," Electron. Lett. 38, 25 (2002)

Chapter 2. Deposition and optimization of a-Se target

Although a-Se based photodetectors were successfully driven by diamond cold cathode in previous studies, photodetection utilizing carrier multiplication was not achieved yet. A reason to this is that the physics of carrier multiplication is still unknown due to a phase transition between amorphous and crystalline selenium: a-Se is known to have at least three different crystal structures at ordinary temperatures and pressures, which are metallic trigonal selenium (t-Se), monoclinic selenium (m-Se) and a-Se. These selenium phases have distinctive optical and electronic properties, and transitions between these phases are induced by thermal/optical stimulations. Therefore it has been difficult to determine the conditions for carrier multiplication in a-Se.

In this chapter, optimization of a-Se target was attempted. Deposition of a-Se film using rotational evaporator is presented in Section 2.1. The degradation of a-Se due to thermal and/or optical stimulation was presented in Section 2.2. An attempt to prevent the degradation is presented in Section 2.3, including stabilization of the film through thermal process based on a previous study on anneal-induced degradation of a-Se film.

2.1. Film deposition using rotational evaporator

The a-Se based photoconductive films were deposited using vacuum evaporation, whose structure is schematically illustrated in Figure 2.1.1 [1]. The substrates were glass faceplates with electric through holes, on which indium-tin-oxide (ITO) transparent conductive films were deposited as back contact. The substrates were fixed on a turntable, which was equipped inside the evaporation system. Underneath the turntable were two molybdenum (Mo) boats that were filled with evaporation source. Two

evaporation sources were used in the system: pure selenium (Se) pellet and powdered arsenic selenide (As_2Se_3), which were separately filled in each Mo boat and evaporated by Joule heat from the boat. The two Mo boats were placed on the opposite side of each other so that the substrate passed above the two sources alternately as the turntable rotated. The film deposited in this way should have multi-layer structure that consisted of Se and arsenic (As) rich Se layers. Incorporation of As was reported to increase the stability of amorphous structure, which could otherwise re-crystallize into trigonal selenium (t-Se) with smaller photoconductivity than amorphous counterparts [2]. The system could equip extra Mo boats for possible chlorine or tellurium (Te) doping, as reported in the literature [3].

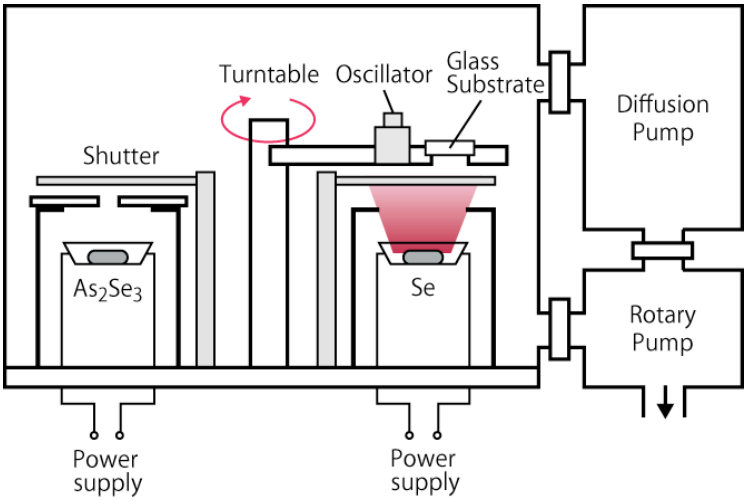

Figure 2.1.1. Schematic diagram of the rotational evaporation system used to deposit a-Se based films [1].

The deposition was performed in the following procedure: once the substrate and evaporation sources were loaded, the system was evacuated to 1.0×10^{-3} Torr using a rotary pump and then connected to a diffusion pump to be evacuated to 1.0×10^{-6} Torr. Prior to the deposition, the evaporation sources were preheated by increasing the electric current through the Mo boats. The current was increased linearly at 10 A/min, up to 40 A

for Se boat and 45 A for As_2Se_3 boat, respectively. The maximum currents were kept for 5 min to ensure the sources to be vaporized, before the shutter above each boat was opened for film deposition. The deposition rate was monitored using a crystal oscillator, which was set alongside with the sample. The deposition was stopped when the oscillator indicated a 60 kHz drop, which corresponded to the film thickness of approximately 2 μm [2]. During the deposition, the rotation speed of a turntable was kept at 80 rpm. After the deposition, the system was kept evacuated for another 1 h for cooling down before the a-Se based films were then taken from the chamber. Following the deposition, the films were mounted on a copper (Cu) base with substrate side down, to be annealed on a hotplate at atmospheric pressure. This annealing process helped a-Se structure shift into a quasi-stable state with stable current-voltage characteristics and resilience to thermal degradation [2]. The optimization of the annealing process is described later in this chapter.

2.2. Degradation of a-Se due to phase shift

As mentioned previously, one of the key factors to demonstrate carrier multiplication is to prevent the degradation of a-Se due to crystallization. Amorphous Se can easily shift into trigonal Se, which is up to 100 times more conductive than its amorphous counterpart. Since a high electric field of ~100 V/μm is reported to induce carrier multiplication [4,5], it is necessary to maintain high-resistive amorphous structure. In this section, phase-shifting nature of a-Se is being investigated. A well-known degradation process is through thermal treatment, but other processes such as photo-irradiation and electron (e-) beam irradiation are briefly explained.

2.2.1. Thermal degradation

The change in photoconductivity due to annealing was characterized by Saito et al., using the a-Se film deposited by rotational evaporation [2]. Figure 2.2.1 shows the apparatus used in the measurement. In this photoconductivity measurement, a-Se films

were annealed at 60–85 °C in 5 °C steps for 5 min each. Figure 2.2.2(a) and (b) show the contact current *versus* applied voltage (I_C-V) characteristics for a-Se films after annealing at 65 °C and 85 °C. The dark current of pure a-Se sample increased after each annealing step and it increased rapidly after 70 °C annealing. The dark current reached up to 10^{-8} A after 85 °C annealing, as shown in Figure 2.2.2(b). It was also reported that the color of a-Se film changed from dark red to black after a 65 °C anneal, and then started to tarnish after a 70 °C anneal. After a 75 °C anneal, the surface changed into a gray, dull metallic color, which was characteristic to t-Se. All the remained black areas turned completely gray after 80 °C, of which transition was also visible in change in photoconductivity.

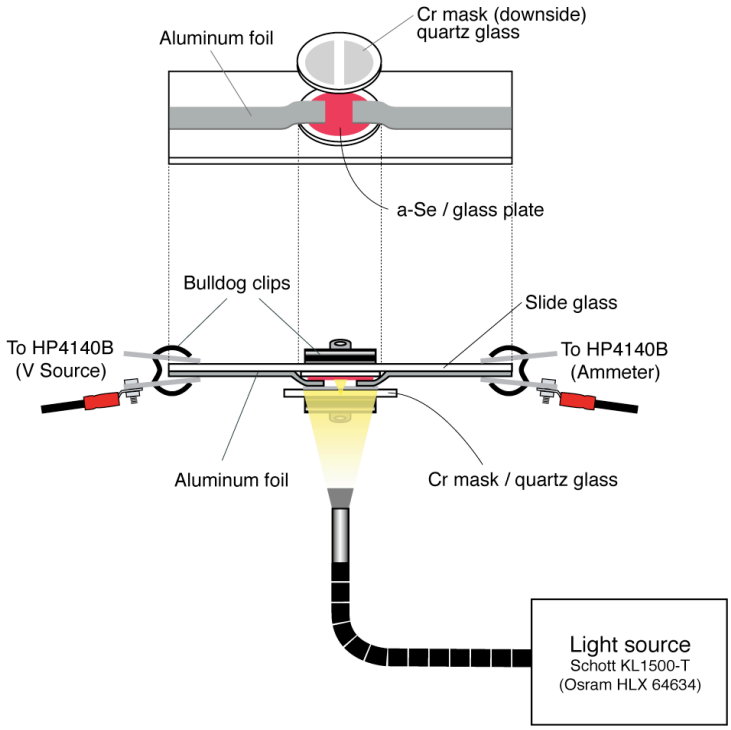

Figure 2.2.1. Schematic diagram of the measurement setup used in ref [2].

In contrast to pure a-Se film, I_C-V characteristics for As_2Se_3 films in Figures 2.2.3(a) and (b) showed much smaller changes throughout the annealing steps: despite the fact where the dark current of a-Se changed drastically, the dark current of a-As_2Se_3 was

stable around late 10^{-13} A for any annealing temperature. The photoconductivity showed a slight change but was still much smaller than a-Se films.

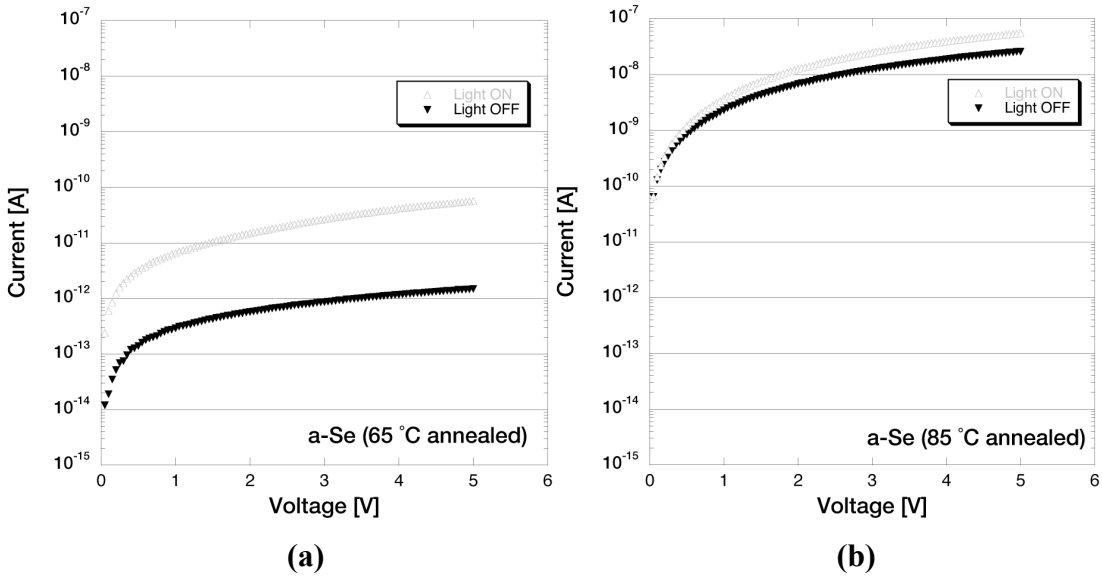

Figure 2.2.2. I_C-V characteristics of a-Se, after annealing at (a) 65 °C and (b) 85 °C. After Saito et al [2].

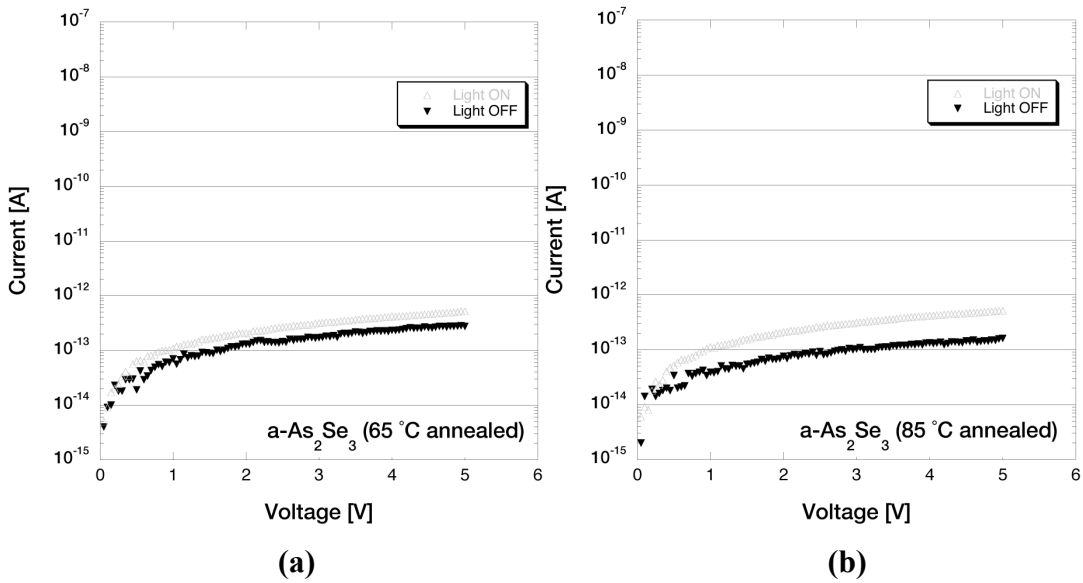

Figure 2.2.3. I_C-V characteristics of a-As2Se3, after annealing at (a) 65 °C and (b) 85 °C. After Saito et al [2].

These results suggested that there was a critical point in annealing temperature, where great changes in the appearance and the photoconductive property could be observed for a-Se films and not for a-As_2Se_3 films. It should be noted that with a certain amount of annealing treatment, where in this case around 65 °C, photoconductivity of the a-Se film improved compared to the as-deposited a-Se sample. It could be explained as follows: the annealing treatment provides thermal energy to cause the reassignment of the disordered selenium atoms in the as-deposited film. The a-Se films could have reached a metastable state at a temperature between 60 °C and 70 °C, when the color of the film was black and just before it started to tarnish, and also before the dark current increased rapidly.

2.2.2. Photo-induced degradation

The degradation of a-Se film was also caused by light illumination. This photo-induced structural change was characterized by Raman spectroscopy. The laser used in Raman spectroscopy can degrade the a-Se by photo-induced crystallization, unless the laser power was optimized for measuring a-Se.

The Raman spectroscopy was carried out using Dilor XY800 Raman system. The laser used for excitation was the 1.92 eV (647.1 nm) emission line of a Kr^+ ion laser. The laser with the power of 18 mW was focused to a spot of approximately 200 μm in diameter on the sample surface. Although the incident laser did not change the film with a single scan, it induced crystallization over time. The time of the laser exposure is proportional to the number of accumulation in the measurement. The Raman spectra of a-Se film with various laser accumulations are shown in Figure 2.2.4. Each spectrum was taken for different spot on the sample, so that the change caused by previous measurement did not affect on the other spectra.

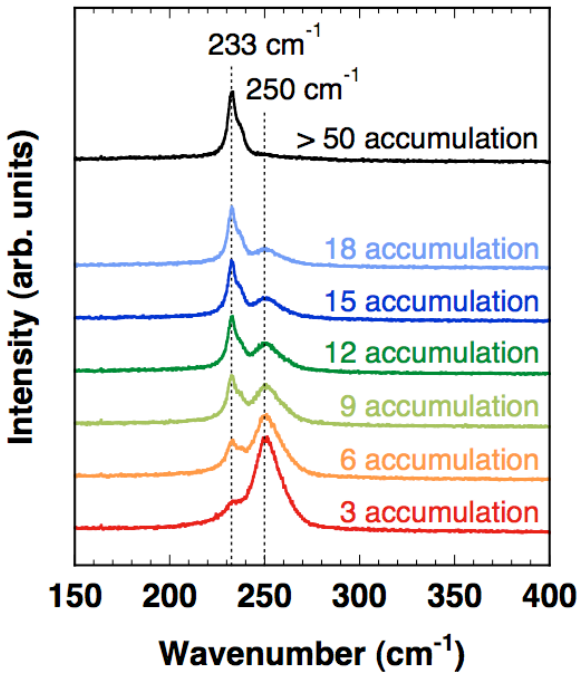

Figure 2.2.4. Raman spectra of a-Se films with different accumulations. The number of accumulation represents total time of laser exposure.

The spectrum taken by 3 accumulations had a broad feature with a peak at 250 cm^{-1}, which is characteristic to a-Se [6]. The intensity of the broad feature decreased as the number of accumulation was increased, whereas a peak appeared at 233 cm^{-1}. This emerging peak could originate in t-Se, whose peak should typically be at 235 cm^{-1} [6]. The peak position was slightly different between pure t-Se and the one in the present study, possibly because of a lattice strain due to the internal stress.

As shown by the Raman spectra, the laser illumination caused a structural change in a-Se, and crystalline t-Se was produced. It was difficult with current setup to tell if this change was induced by pure optical stimulation or by thermal stimulation caused by the laser, since the measurement setup did not equip a cooling facility. In either case, crystallization caused by light illumination can be critical for a-Se based photodetectors, since it may determine the lifetime of a photodetector.

2.2.3. Degradation due to e-beam irradiation

The degradation of a-Se film was also observed when a diode-structured photodetector, such as the one presented in Section 1.4.1, was operated at either high voltage or high emission current. In such cases, a spot-like degradation appeared on the surface of a-Se film, as presented in Figure 2.2.5 (b). Such spot-like degradation can be prevented by reducing the operation voltage and current of a photodetector, which is presented in detail in Chapter 4.

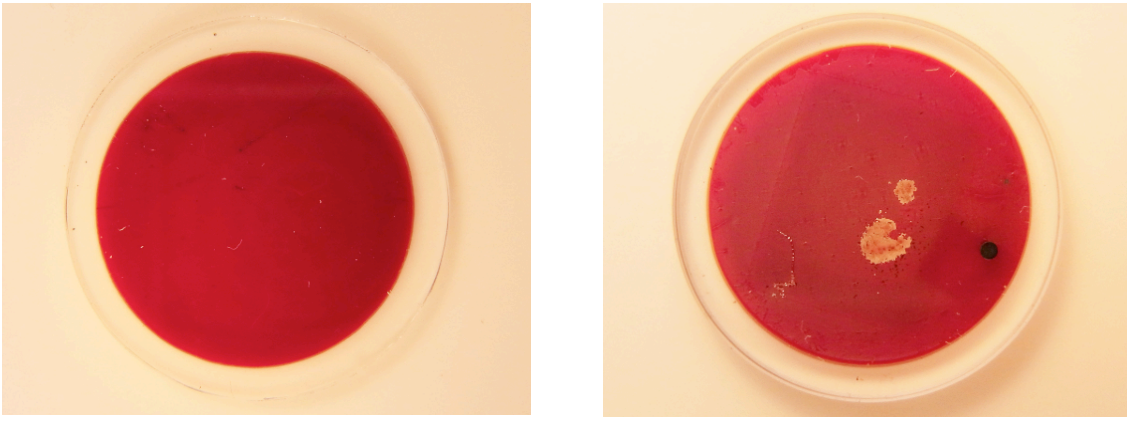

(a) (b)

Figure 2.2.5. Pictures of (a) as-depo a-Se film and (b) a-Se target for a photodetector after e-beam bombardment.

2.3. Optimization of a-Se film

As mentioned in the previous section, a-Se can shift into crystalline selenium or other quasi-stable state, by stimulations such as annealing, light irradiation and e-beam irradiation. It was also mentioned in Section 2.2.1 that anneal-induced degradation could be prevented by incorporating As into a-Se film. However, As incorporation also decreased the photoconductivity of a-Se, therefore, the amount of As incorporation must be optimized. In this section, the stabilization effect of As was investigated by comparing critical phase transition temperature of pure a-Se and As-incorporated a-Se film. The

As-incorporated films were deposited with small amount of As_2Se_3 incorporated through the rotational evaporation. The films were then characterized using Raman spectroscopy, in order to find the temperature at which phase transition occurs.

The a-Se films with different As content were measured by Raman spectroscopy, with the samples annealed between each measurement. The annealing temperature was increased from 45 ^{o}C by 5 ^{o}C step, and changes in the spectra were compared for different annealing temperatures. The measurement system used in this study was same as the one presented in Section 2.2.2. The measurement was conducted in a ultra high vacuum chamber, and the measurement and annealing were conducted without breaking the vacuum. The excitation laser was Kr^{+} ion laser operated at 18 mW, which is focused to a spot of approximately 200 μm in diameter on the sample surface. The Raman spectra were taken for different spots of the samples. All Raman spectra were recorded in a backscattering geometry. A detailed description of this set-up was given in [2].

Figure 2.3.1 (a) and (b) illustrate the Raman spectra for the film with and without As incorporation, respectively. The relatively broad feature with a peak at 250 cm^{-1} was characteristic to a-Se, and the sharp peak at 233 cm^{-1} represented t-Se, which was produced by crystallization. The results shown in Figure 2.3.1 demonstrated that the a-Se peak in the As-incorporated film remained even after 105 ^{o}C annealing. In contrast, Raman spectrum for the pure a-Se film showed that the a-Se peak decreased rapidly after 85 ^{o}C annealing and almost disappeared after 105 ^{o}C annealing. The crystalline t-Se peak at 233 cm^{-1} appeared and dominated the spectrum after 120 ^{o}C accumulations, meaning that the film had almost entirely crystallized into t-Se.

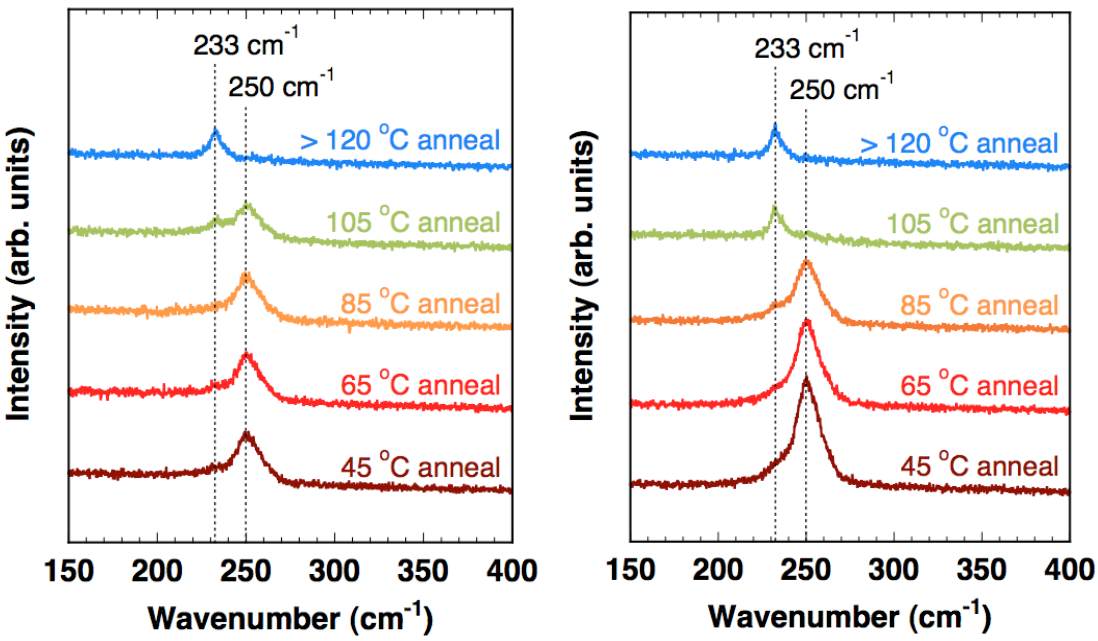

(a) (b)

Figure 2.3.1. Raman spectra of the deposited films after annealing: (**a**) with As incorporation and (**b**) pure a-Se without As incorporation.

The Raman spectra showed that a critical phase transition temperature of a pure a-Se is approximately 65 °C, while it was increased to 85 °C for the As incorporated films. Annealing at higher temperatures could cause the film to recrystallize into trigonal selenium (t-Se), which was metallic and had lower photoconductivity than a-Se. The higher phase transition temperature suggested that the structure of this film is more resilient against phase transition caused by thermal stimulation.

Now that the stabilization effect of As incorporation has been proven, the contact current *versus* applied voltage (I_C-V) characteristics is examined in order to observe the effect of the As incorporation on the electric properties. The I_C-V measurement results for the both a-As_2Se_3 film and As-incorporated a-Se are shown in Figure 2.3.2. The dark current of the As_2Se_3 film is smaller than that of the As-incorporated a-Se film, although it shows less to no change between the dark current and the photo-current. The clear increase

of the photo-current in As-incorporated film proves that this film achieved increased stability while maintaining good photoconductivity.

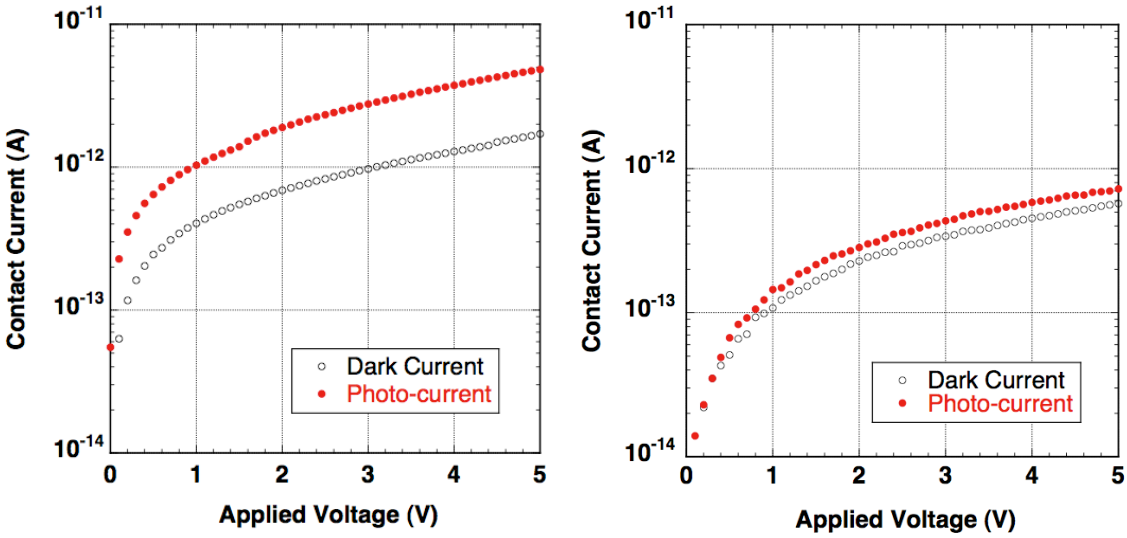

(a) (b)

Figure 2.3.2. I_C-V characteristics of (**a**) a-Se with small As incorporation and (**b**) a-As_2Se_3.

As a summary, degradation of a-Se film due to the transition into t-Se has been extensively studied: since such transition is caused by various stimulations such as annealing, light illumination and e-beam bombardment, the stabilization of a-Se target is one of the key technologies in the a-Se based photodetector. Incorporation of amount of As into a-Se film has been proven to increase the stability of the film, while excessive As incorporation is reported to decrease the photoconductivity [2]. The next step is to operate this optimized film in carrier multiplication mode, which is presented in detail later, in Chapter 4.

References

[1] I. Saito, W. Miyazaki, M. Onishi, Y. Kudo, T. Masuzawa, T. Yamada, A.T.T. Koh, D.H.C. Chua, K. Soga, M. Overend, M. Aono, G.A.J. Amaratunga, and K. Okano, "A transparent ultraviolet triggered amorphous selenium p-n junction," Appl. Phys. Lett. 98, 152102 (2011)

[2] I. Saito, K. Oonuki, T. Yamada, M. Aono, T. Butler, N. L. Rupesinghe, G. A. J. Amaratunga, W. I. Milne and K. Okano, "Anneal-Induced Degradation of Amorphous Selenium Characterized by Photoconductivity Measurements," Jpn. J. Appl. Phys. 44, L334-L337 (2005)

[3] M. Kubota, "Progress in Development of HARP Imaging Device and Its Application [in Japanese]," Journal of the Institute of Image Information and Television Engineers, Vol. 64, No. 3, 289-292(2010)

[4] K. Tanioka, J. Yamazaki, K. Shidara, K. Taketoshi, T. Kawamura, S. Ishioka and Y. Takasaki, "An Avalanche-Mode Amorphous Selenium Photo- conductive Layer for Use as a Camera Tube Target," IEEE Electron Device Lett. EDL-8, 9, 392-394 (1987)

[5] S. Kasap, J. A. Rowlands, S. D. Baranovskii and K. Tanioka, "Lucky drift impact ionization in amorphous semiconductors," J. Appl. Phys. 96 2037 (2004)

[6] I. Saito, T. Masuzawa, Y. Kudo, S. Pittner, T. Yamada, A. T.T. Koh, D. H.C. Chua, Y. Mori, D. R.T. Zahn, G. A.J. Amaratunga and K. Okano, "Durability and photo-electric characteristics of a mille-feuille structured amorphous selenium (a-Se)–arsenic selenide (As2Se3) multi-layered thin film," Journal of Non-Crystalline Solids, 378, 96 (2013)

Chapter 3. Synthesis of nitrogen(N)-doped diamond film and its electron emission mechanism

In this chapter, deposition of nitrogen (N)-doped diamond thin films is presented along with their field emission properties. Section 3.1 describes deposition procedure of diamond thin film using chemical vapor deposition (CVD). In this study, dimethylurea was introduced as a dopant for N-doping, in addition to the previously reported dopant, urea. The films were then characterized using scanning electron microscope (SEM), X-ray diffraction (XRD) and Raman spectroscopy, of which results were presented in Section 3.2. The field emission properties of N-doped diamond thin films were discussed in section 3.3, where correlation between N-doping and field emission mechanism was investigated.

3.1. Synthesis of nitrogen-doped diamond thin film

Nitrogen (N)-doped diamond films were grown using hot filament chemical vapor deposition (HFCVD) technique [1]. Chemical vapor deposition of diamond thin film was developed in the 1980s, and became popular due to its low cost and ease of experiments compared to high-pressure, high-temperature (HPHT) deposition [2].

An experimental setup of HFCVD is schematically depicted in Figure 3.1.1. A mixture of hydrogen (H_2) and reactant gas was introduced into the chamber, while a rotary pump displaced the gas in the chamber to balance the inside pressure at 100 Torr. The molecular bonds of the introduced gas were broken by the thermal energy of the heated tungsten filament, and reactant species containing carbon atoms were deposited on the substrate located just below the filament. Although the reactant species could contain sp^2

and sp^3 carbon radicals, sp^2 fraction was selectively removed from the surface due to a different etching rate of sp^2 and sp^3 carbon by hydrogen radicals [2]. As a result, sp^3 carbon atoms were accumulated on the substrate and forms diamond thin film. Although there were other CVD techniques for diamond films, such as plasma-enhanced CVD (PECVD) and thermal CVD [2], HFCVD was chosen due to its simplicity and capability of N-doping. A nitrogen concentration of 10^{20} cm^{-3} was reported only for HFCVD diamond [1], whereas such a heavy N-doping was thought to be a key for electron emission under low electric field.

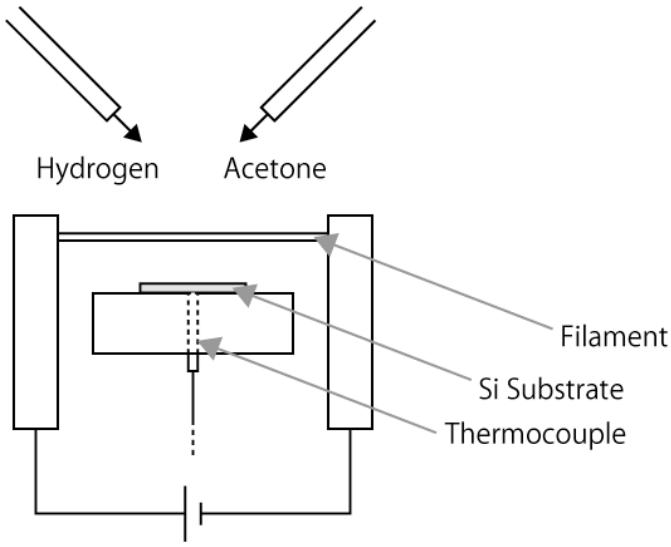

Figure 3.1.1. Schematic diagram of HFCVD system.

Another key factor to obtain heavily N-doped diamond was the dopant incorporated in the reactant gas. The reactant gas was prepared as follows [1]. Acetone [$(CH_3)_2CO$] was the source gas for growing diamond and N-dopant is dissolved into acetone. Two types of N-dopant were selected in this study: urea [$(NH_2)_2CO$] and dimethylurea(DMU) [$(CH_3NH)_2CO$]. Urea was chosen for the dopant because it was the "magic recipe" for a heavily N-doped diamond, which exhibited an electron emission

under extremely low electric field in the literature [1]. Since urea was not soluble in acetone, it was first dissolved in methanol [CH_3OH] to form a saturated solution and then diluted to l/10 with acetone. This reactant solution was then vaporized and used as the reactant gas. The nitrogen concentration in the reactant gas was estimated from the weight of the source materials: the molar fraction of nitrogen was 30 % of carbon, assuming that all chemical compounds had the same vapor pressure.

Although N-doped diamond films deposited using urea as N-source were reported to exhibit electron emission under extremely low electric field [1], the deposition procedure could have reproducibility issue, since urea suffered re-crystallization in acetone-diluted solution, which could result in limited control of nitrogen incorporation. In order to improve the reproducibility of N-doping, a new doping method was proposed by Kudo et al. using DMU as dopant [3]. As mentioned earlier, urea recrystallized before and during fabrication because it was not soluble to acetone. Urea needed to be dissolved into methanol, and then diluted by acetone to create the reactant solution, while DMU dissolved directly into acetone and incorporation of methanol was not necessary.

The experimental conditions for HFCVD process were as follows using the setup apparatus shown in Figure 3.1.2. The filament temperature measured by an optical pyrometer was 2,300 °C and the substrate temperature measured by a thermocouple was 850 °C. The reactant gas ratio against H_2 was 0.6 vol.% and the flow rate of the gas was 100 cc/min. Films were grown for 2 h on 2.5 × 2.5 mm n-type (100) Si substrates, the surfaces of which were scratched with diamond paste with grain size of 1 μm in order to obtain high nucleation density for a continuous film. In this study, three samples with different dopant concentrations were prepared for comparison: the molar fraction ratio of nitrogen/carbon (N/C) in these samples were estimated to be 10 ppm, 100 ppm, and 1,000 ppm, respectively.

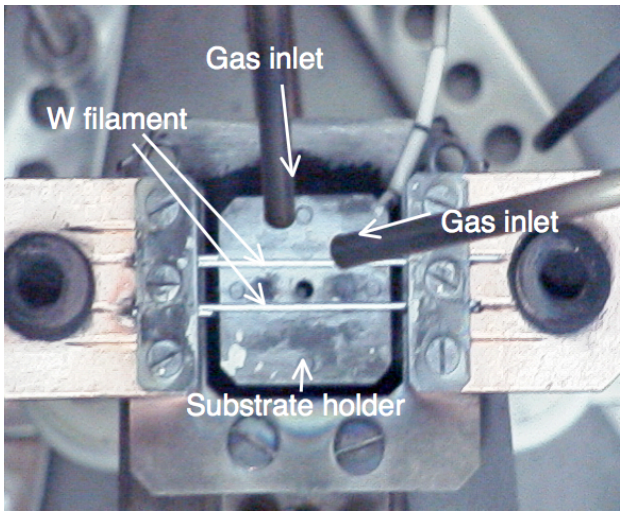

Figure 3.1.2. Top view of HFCVD apparatus used in this study

3.2 Characterization of the deposited film

The morphological and crystallographic properties of the films deposited by CVD were characterized using scanning electron microscope (SEM) and X-ray diffraction (XRD) as well as Raman spectroscopy.

The morphology of the deposited films was characterized using JEOL JSM-5510 SEM system. The films were mounted on a metal template and introduced to the observation chamber, which is pure-evacuated by rotary pump and then connected to a diffusion pump to be evacuated for 1 hour. The acceleration voltage of scanning electron beam was set to 10 kV and secondary electron image was collected. Figure 3.2.1 (a)-(c) show the SEM images of the films with different N/C ratio. The images showed that the deposited films were polycrystalline film with average grain size of ~5 μm. The SEM images showed that the difference in N/C ratio did not lead to any noticeable change in morphology.

a) 10 ppm

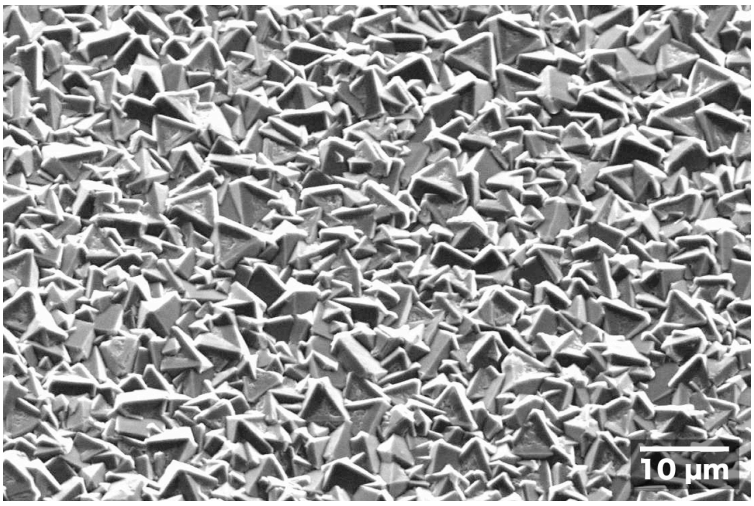

b) 100 ppm

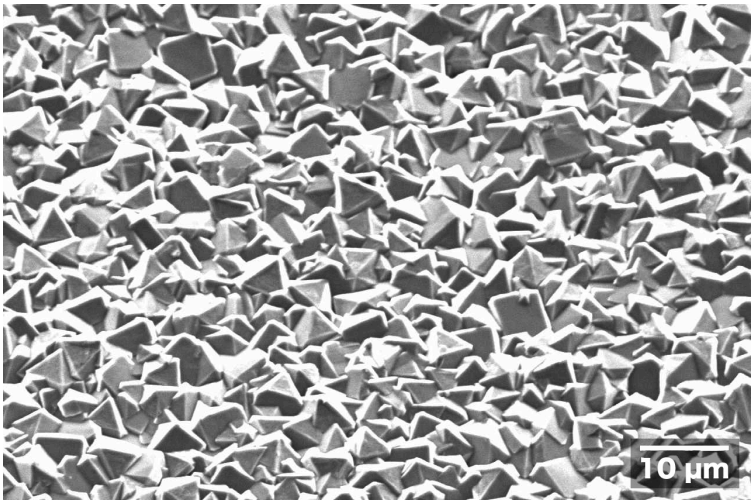

c) 1,000 ppm

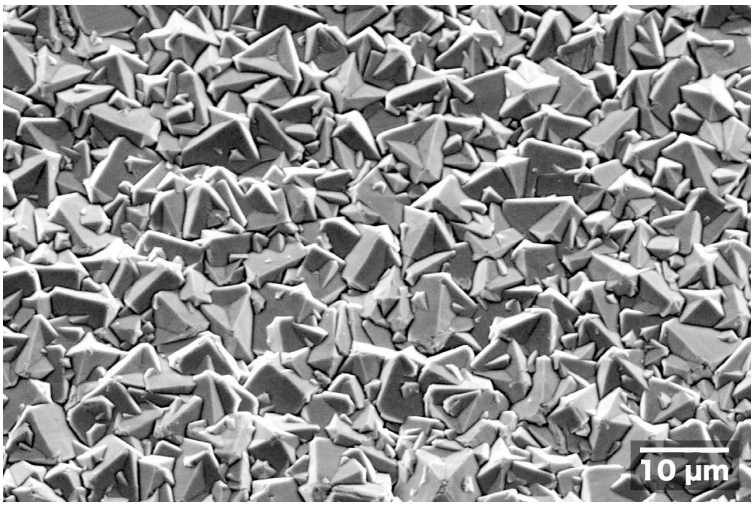

Figure 3.2.1. SEM image of the CVD-grown films doped with a) 10 ppm, b) 100 ppm, and c) 1,000 ppm dimethylurea.

Following the SEM observation, the crystal structures of the films were characterized by XRD in order to confirm that these films were diamond. The lattice constants and crystal orientations were compared between samples with different N/C ratio to investigate the change in crystal lattice due to nitrogen incorporation.

In XRD, X-ray with a known wavelength was irradiated on the sample, and the diffracted X-ray was detected in order to determine the lattice parameter of the sample. When an X-ray of wavelength λ is irradiated on a sample surface, the X-ray is diffracted by the crystal planes of the sample, and the diffracted X-ray is intensified in the angle determined by the Bragg condition:

$$2d\sin\theta = n\lambda \qquad (3.2.1)$$

where θ is the angle relative to the incident X-ray, d is the lattice spacing of the material and n is a natural number representing a factor of multiplication. The Bragg condition suggests that by investigating θ, one can obtain the information of the lattice spacing d, which is compared to the value of known materials to determine the structure of an unknown sample.

The XRD measurement was conducted by θ-2θ method. The sample was rotated by an angle θ relative to the incident X-ray, while the X-ray detector was scanned in the same direction by 2θ. As a result, intensity of the diffracted X-ray was plotted in terms of the angle 2θ, which represents the lattice spacing of the sample. A characteristic X-ray of Cu Kα (1.5443 Å) was used as the incident X-ray. Three types of samples with different dopant concentration were prepared in order to investigate the effect of N-doping. N/C ratios of these samples were 1,000 ppm, 100 ppm and 10 ppm, respectively.

Figure 3.2.2 shows the XRD spectra for the deposited films with different N/C ratios. Multiple peaks were observed in the spectra, which represented the diffraction of different lattice planes: since the deposited films were polycrystalline, the films should

contain various plane directions, which resulted in XRD spectra similar to those of powder samples. In order to interpret the peak positions in the XRD spectra, reference values of *d* were taken from a literature [4,5]. These values were used to estimate the peak positions of natural diamond using Eqn. 3.2.1. The reference values of *d* and the peak position for natural diamond are listed in Table 3.2.1.

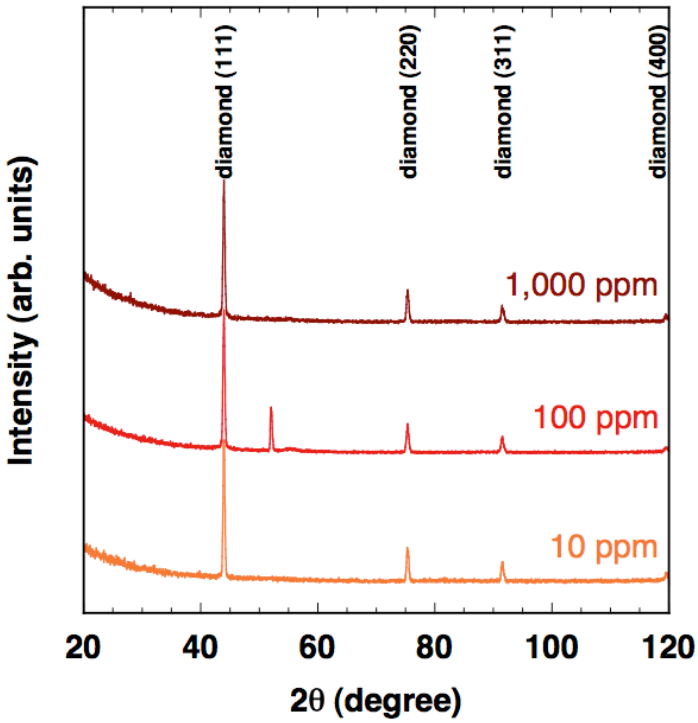

Figure 3.2.2. XRD spectra of the CVD-grown films with different N/C ratios.

The peak positions in Figure 3.2.2 showed a good agreement with the estimated diffraction peaks of diamond (111), (220), (311) and (400) surfaces. One unidentified peak found in 52.04 degree 2θ for 100 ppm film could originate in a contaminant, but overall the samples were confirmed to be diamond films.

Another key parameter for analyzing XRD spectra is lattice constant. Since diamond has cubic lattice, the lattice constant *a* can be estimated using following equation:

$$\frac{1}{d^2} = \frac{1}{a^2}\left(h^2 + k^2 + l^2\right) \qquad (3.2.2)$$

where a is a lattice constant and h, k, l are a set of natural numbers called *plane indices*, which determine a lattice plane. The lattice constant estimated from the peak positions in XRD spectra are shown in Table 3.2.2, which showed a good agreement with that of natural diamond, 3.5667 Å [4,5]. However, no noticeable change in the lattice constant was found depending on the N/C ratio.

Table 3.2.1. Reference values of d for natural diamond and XRD peak value estimated for each d [4,5].

hkl	d (Å)	2θ (degree)
111	2.06	44.0
220	1.261	75.52
311	1.0754	91.781
400	0.8916	120.0

Table 3.2.2. The peak values taken from XRD measurements, as well as the lattice spacing and lattice constant estimated from the Eqn. 3.2.2.

10 ppm

hkl	2θ (degree)	d (Å)	a (Å)
111	44.00	2.058	3.564
220	75.28	1.262	3.570
311	91.60	1.075	3.566
400	119.52	0.892	3.569

100 ppm

hkl	2θ (degree)	d (Å)	a (Å)
111	43.96	2.058	3.568
220	75.36	1.261	3.567
311	91.56	1.076	3.568
400	119.48	0.893	3.570

1,000 ppm	*hkl*	2θ (degree)	*d* (Å)	*a* (Å)
	111	43.96	2.060	3.568
	220	75.36	1.261	3.567
	311	91.48	1.076	3.570
	400	119.48	0.893	3.570

The ratio of the peak intensity for each of the samples was then compared to characterize lattice-preferred orientation. The relative peak intensities obtained from the XRD spectra are listed in Table 3.2.3, taking (111) peak to be 100. The reference values taken from the literature were those of powdered natural diamond, which suggested that the sample had no preferred orientation: one could assume that all plane direction existed in the same amount. The relative peak intensities for 10 ppm film were almost same as the reference values, which suggested that the film has no preference in orientation. On the contrary, the relative peak intensities for 100 ppm and 1,000 ppm films showed that the intensity of (220), (311) and (400) peaks are lower than the reference value. This tendency suggested that these films contained more (111) surfaces than those of the reference sample, i.e. the films were oriented in (111) direction.

Table 3.2.3. A list of relative intensity for each of the XRD peaks. The reference values are those of a powdered natural diamond presented in the literature [4,5].

hkl	Reference	1,000 ppm	100 ppm	10 ppm
111	100	100	100	100
220	25	24.0	21.2	25.5
311	16	13.4	12.4	15.6
400	8	7.3	4.8	8.2

Although XRD measurement confirmed that the CVD-grown films were diamond, the content of amorphous carbon (a-C) was unidentified, since the XRD was not sensitive to a-C. In order to evaluate the a-C component, Raman spectroscopy was conducted. In this measurement, microscopic Raman spectrometer was used in backscattering configuration. An Ar^+ laser with a wavelength 488 nm was irradiated on the sample, and the scattered light was collected using CCD. Figure 3.2.3 shows the Raman spectra obtained for the CVD-grown films with 10 ppm, 100 ppm and 1,000 ppm. The peak at 1,332 cm^{-1} is characteristic to a diamond, whereas the broad feature having peak at 1,550 cm^{-1} originated in a-C [6]. The present result suggested that the samples were diamond with only little a-C or graphitic component.

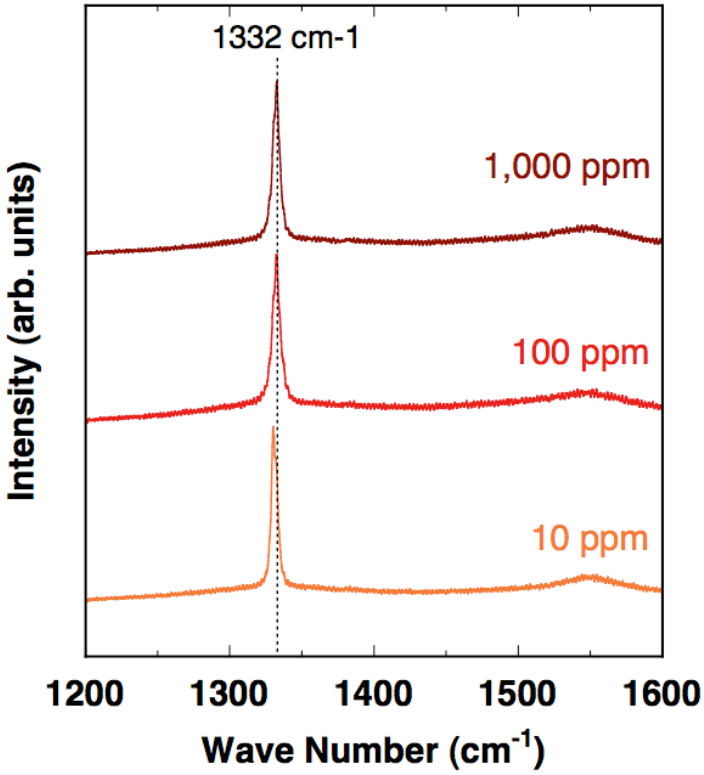

Figure 3.2.3. Raman spectra of the CVD-grown films with different N/C ratios.

The crystal perfection of the diamond film was compared between films with different N/C ratio in order to investigate the effect of nitrogen doping. Table 3.2.4 (a) shows the peak position and full-width at half-maximum (FWHM) of the diamond peaks. The FWHM represents a crystal perfection of the film, and typical values of CVD-grown diamond were between 5-10 cm^{-1}. As listed in Table 3.2.4 (a), the FWHM of the deposited films were within the range 5.0-6.0 cm^{-1}, suggesting that the obtained films were diamond with good crystal perfection. FWHM of 10 ppm film was smallest, which means that this sample had highest crystal perfection among these three.

One may note that the peak position of 10 ppm sample was 1,330.2 cm^{-1}, which was slightly shifted from the peak position of natural single-crystal diamond. The peak position for a natural diamond was 1,332 cm^{-1} according to the literature [6]. The shift in the peak position could be explained by a strain in the crystal. Since the Raman shift is determined by the vibrational mode of crystal lattices, any strain in the lattice could cause a change in the vibration.

To summarize this section, the films grown by CVD were characterized using SEM, XRD and Raman spectroscopy, and it was found that the obtained films were polycrystalline diamond with only few a-C components. The next step is to characterize their field emission property so that the films are optimized for a cold cathode that drives the a-Se based photodetector.

Table 3.2.4. A list of relative intensities of diamond peaks and a-C peaks.

a)

	Peak position (cm^{-1})	FWHM (cm^{-1})
10 ppm	1330.2	5.0
100 ppm	1333.6	6.0
1,000 ppm	1333.6	5.8

b)

	Diamond peak	a-C peak
10 ppm	100	22.6
100 ppm	100	29.7
1,000 ppm	100	25.2

3.3 Correlation between C-N bond and threshold field of N-doped diamond [7]

N-doped diamond thin films between the conventional urea doped film and the newly introduced DMU doped film are investigated in terms of electron emission property and their composition. DMU doped diamond samples, which required relatively high extraction voltage for field emission, were deliberately chosen for the comparison of its distinctive characteristics. Three types of samples were prepared for the comparison: one was reference sample using urea as dopant, while the other two were synthesized using DMU as dopant with different concentrations. The nitrogen/carbon (N/C) ratio of the reactant gas were calculated and approximated to be 1000 ppm and 10 ppm, respectively.

The field emission properties were characterized by emission current *versus* anode voltage (*I-V*) measurements and the barrier height was calculated. Figure 3.3.1 shows the setup used for *I-V* measurement. The anode was electrochemically etched tungsten needle, which could scan the surface of the diamond film in x-y direction. The anode-cathode distance could also be varied in 1 μm step without breaking the vacuum.

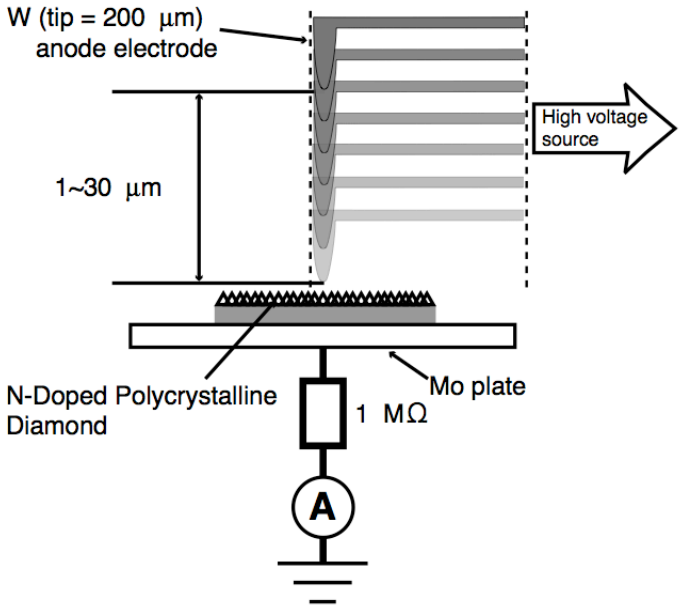

Figure 3.3.1. A schematic diagram of the field emission measurement system after ref [7].

The *I-V* characteristic of the three samples, with anode-cathode distance varied from 1 μm to 30 μm, are shown in figure 3.3.2 (a)-(c). It was apparent that the samples doped with DMU required larger extraction voltage compared to the reference sample doped with urea. In addition, the extraction voltage was higher for the sample with lower DMU concentration within the reactant solution.

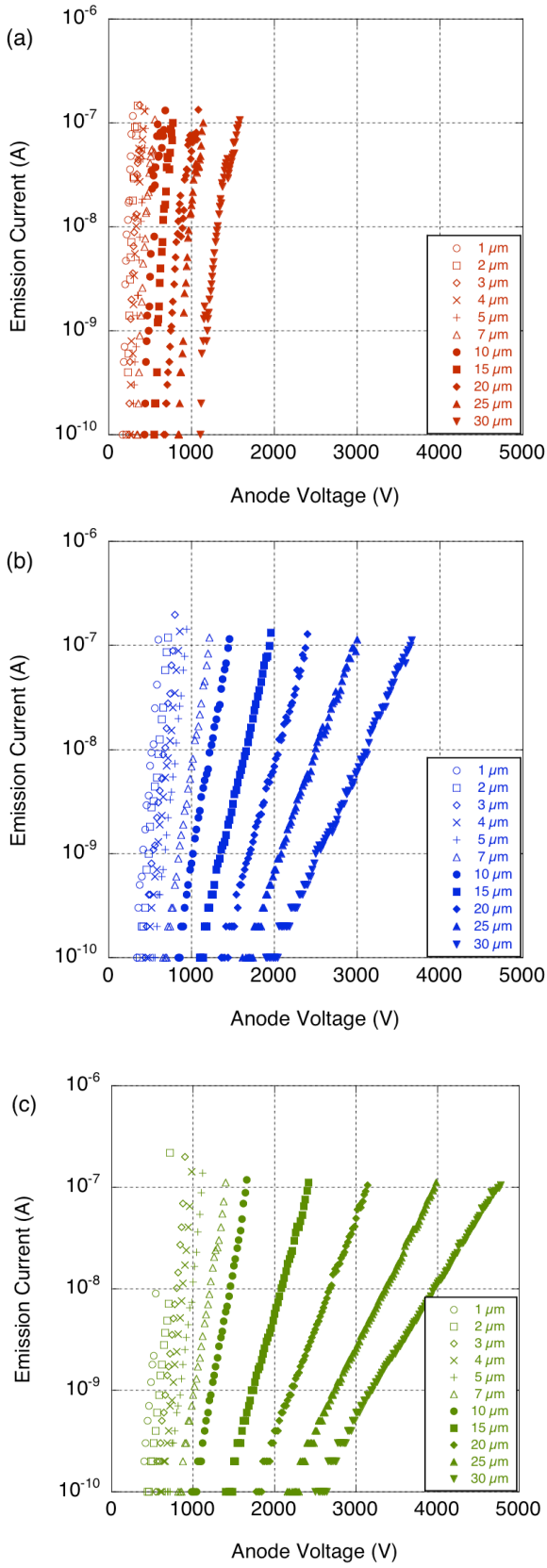

Figure 3.3.2. *I-V* characteristics of (a) reference sample doped with urea, the sample doped with (b) DMU 1000 ppm and (c) DMU 10 ppm [7].

In order to further analyze the field emission property of the diamond films, Fowler-Nordheim (F-N) plots were obtained from the *I-V* characteristics. The F-N plots for all the samples were fitted into a straight line with a negative slope, as shown in Figure 3.3.3, which was typically observed for field emission under the existence of a potential barrier between the surface and the vacuum [8]. According to the standard F-N theory, the slope of the F-N plot depends on both the potential barrier height and the field enhancement factor (β) [8]. The field enhancement factor indicates the field concentration at the point of field emission, and is related to the curvature of the electron emitter surface and the distance between the anode and the cathode [9]. Surface morphology observation using a scanning electron microscope (SEM) showed that there was no notable difference between each surfaces. Therefore, the field enhancement factors for each sample were assumed to be nearly equal, and the barrier height should be proportional to the slope of the F-N plot. The ratio of the barrier height is represented by

$$\frac{\phi_2}{\phi_1} = \left(\frac{\Delta_2}{\Delta_1}\right)^{2/3}$$

where ϕ_1 and ϕ_2 are the barrier height and Δ_1 and Δ_2 are the slopes of the F-N plot for the samples compared. The slopes of the F-N plot, as well as calculated barrier height ratio, were shown in Table 3.3.1. It was obvious that the calculated barrier heights were larger for the DMU samples. Moreover, the barrier was slightly higher when the nitrogen concentration of the reactant solution was lower.

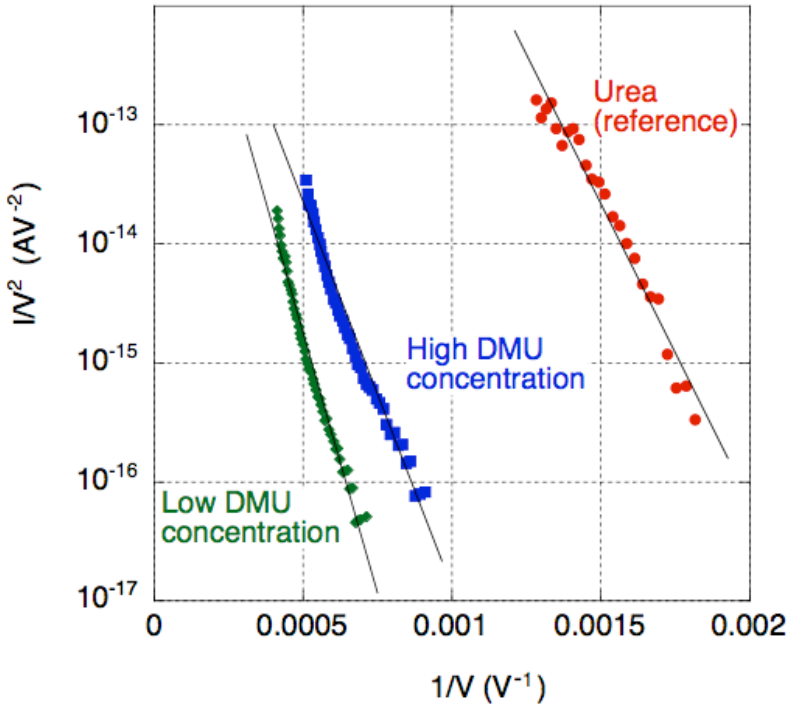

Figure 3.3.3. F-N plots of the reference sample doped with urea, the sample doped with DMU 1000 ppm, and the sample doped with DMU 10 ppm. The anode-cathode distance was 15 μm [7].

Table 3.3.1. The slope of the F-N plot and the barrier height ratio of N-doped diamond films with different doping conditions [7].

Samples	Slope of F-N plot	Barrier height ratio
Reference	-2200 ~ -19000	1
DMU 1000 ppm	-4000 ~ -24000	1.1 ~ 1.5
DMU 10 ppm	-5400 ~ -31000	1.4 ~ 1.8

The ratio of the potential barrier height was then evaluated from the electric field in the vacuum [10], which was calculated from a threshold voltage *versus* anode-cathode distance (V-d) plot. A V-d plot was obtained by following steps. First, the *I-V* characteristics were measured for several anode-cathode distances. Second, the threshold

voltage, in this case, the voltage required to extract 1 nA of emission current, was determined for each anode-cathode distance. These threshold voltages (V) were then plotted with respect to anode-cathode distance (d), which resulted in a V-d plot. The obtained V-d plot is shown in Figure 3.3.4. By vertically flipping the plot, one can obtain the potential profile within the vacuum during field emission [11,12].

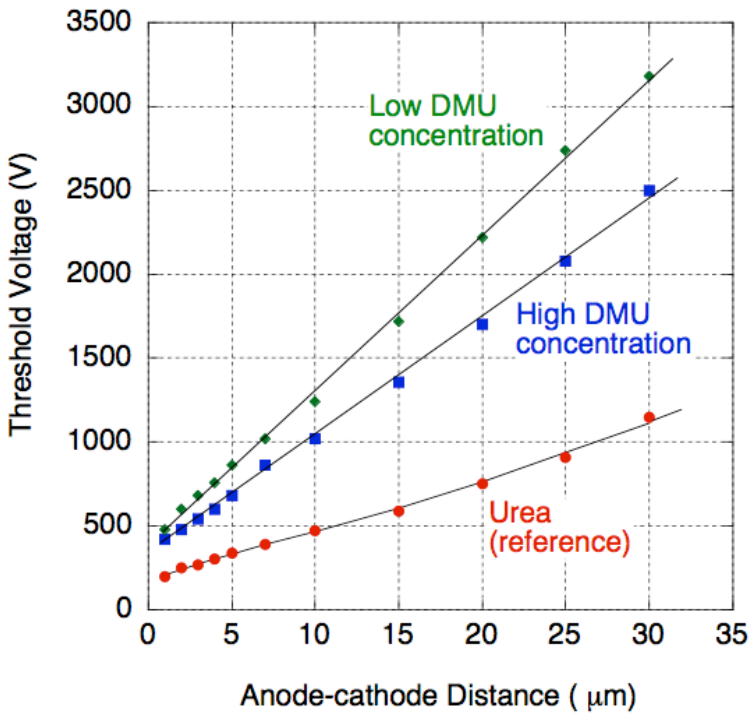

Figure 3.3.4. V-d plots of the reference sample doped with urea, the sample doped with DMU 1000 ppm, and the sample doped with DMU 10 ppm [7].

The average electric field can be estimated from the slope of the linear fit. The standard F-N theory gives that the tunneling probability is determined by the potential barrier height and the electric field at the material surface. Since the tunneling probability is represented by the field emission current, the height of the potential barrier can be compared by the electric fields estimated from the V-d plots. Assuming that the field enhancement factors are nearly the same for all samples, the ratio of the electric field is

proportional to the ratio of the potential barrier height by the power of 3/2. Thus

$$\frac{\phi_2}{\phi_1} = \left(\frac{F_2}{F_1}\right)^{2/3}$$

where F_1 and F_2 are the electric field at the surface of the diamond films. The estimated electric field and barrier height ratio for each of the samples were written in Table 3.3.2. In correlation to the V-d results, it was found that the barrier height for the samples doped with DMU were higher than the one doped with urea. Also, the barrier height is lower for the samples with higher nitrogen concentration. The tendencies in both of the barrier height ratio derived from F-N plot and V-d suggested that there was a significant difference in barrier heights, between the samples doped with DMU and the one doped with urea. Also, a slight difference in the barrier heights was found between samples doped with different DMU concentration, although the difference was not as large as the difference in DMU concentration (~100 times).

Table 3.3.2. The electric field across the vacuum and the barrier height ratio, which were calculated from the V-d plot of N-doped diamond films with different doping condition [7].

Samples	Electric field	Barrier height ratio
Reference	30.6 V/μm	1
DMU 1000 ppm	70.6 V/μm	1.75
DMU 10 ppm	92.7 V/μm	2.09

The electron affinities of the samples were then estimated by UPS measurement, expecting that the difference in the barrier height originated in the difference in the electron affinity. A helium discharge lamp (hν= 21.2 eV) operated at a discharge current of 45 mA was used for the UV light source. The He I is suitable to excite electrons over the

optical band gap of the diamond (5.47 eV), which enables the investigation of the band structure of the diamond films. However, the electron affinities estimated from the UPS spectra are 0.4 ± 0.1 eV for all the samples. The UPS spectra of the samples with different doping conditions are illustrated in Figure 3.3.5. Therefore, the difference in the barrier height cannot be explained by the difference in electron affinity. The next thing expected to make the difference was the nitrogen incorporation.

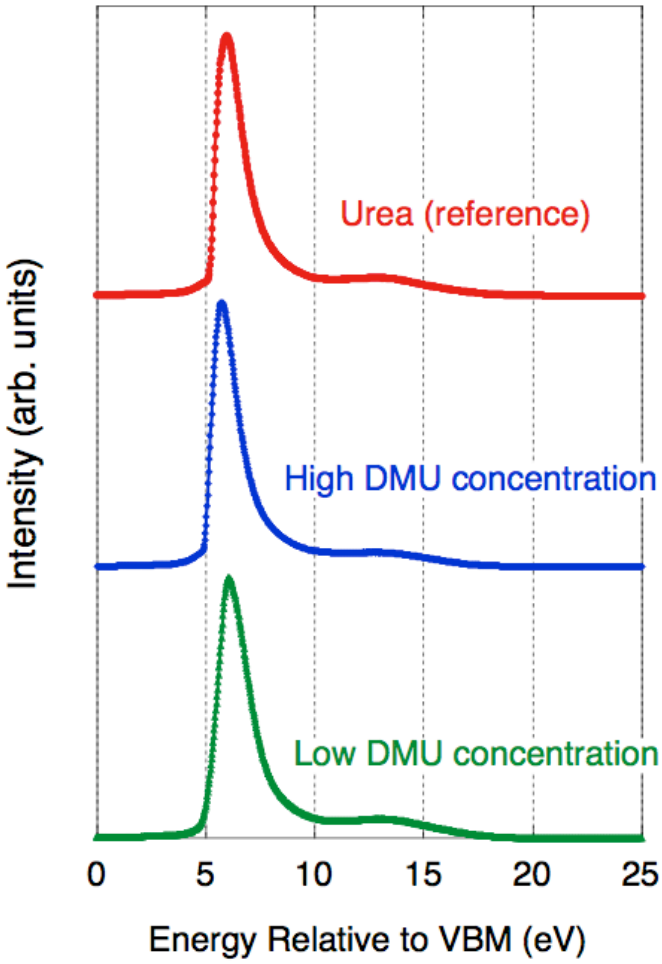

Figure 3.3.5. UPS spectra of the reference sample doped with urea, the sample doped with DMU 1000 ppm, and the sample doped with DMU 10 ppm [7].

TOF-SIMS was carried out to determine the nitrogen ingredients in the samples. TOF-SIMS was specifically selected over dynamic SIMS so that the analysis did not break the bonds incorporated with the nitrogen atom, which could be used to discuss how the

nitrogen was doped. A gallium ion gun was used to induce the secondary ion from the sample surface. The acceleration voltage was 25 kV, and ion current was 2.00 pA. A cesium ion gun was used to sputter the sample. As shown in Figure 3.3.6, TOF-SIMS spectra indicated that the signal representing carbon-nitrogen conjugate (C-N) for the urea doped film was up to 30 times larger than those of the DMU samples. It should also be noted that the C-N signals of the two DMU samples showed about the same intensity. The same C-N signal intensities of the two DMU samples might be related to the distribution of C-N bonds within the bulk. The speculated model was as follows. If the nitrogen atoms were assumed to be concentrated like a cluster in the bulk, TOF-SIMS spectra might indicate smaller C-N concentration than average C-N concentration in the film, unless the cluster was specifically measured. Also, segregation of nitrogen could cause variation of resistivity across diamond film. Since the high resistivity was considered to be the key to achieve low-threshold emission [12], variation of resistivity might disrupt the field emission properties of the film. In order to further investigate the relationship between C-N bond and field emission property, the next step would be to conduct a TOF-SIMS measurement on heavily N-doped diamond doped with both urea and DMU that were confirmed to exhibit low voltage emission.

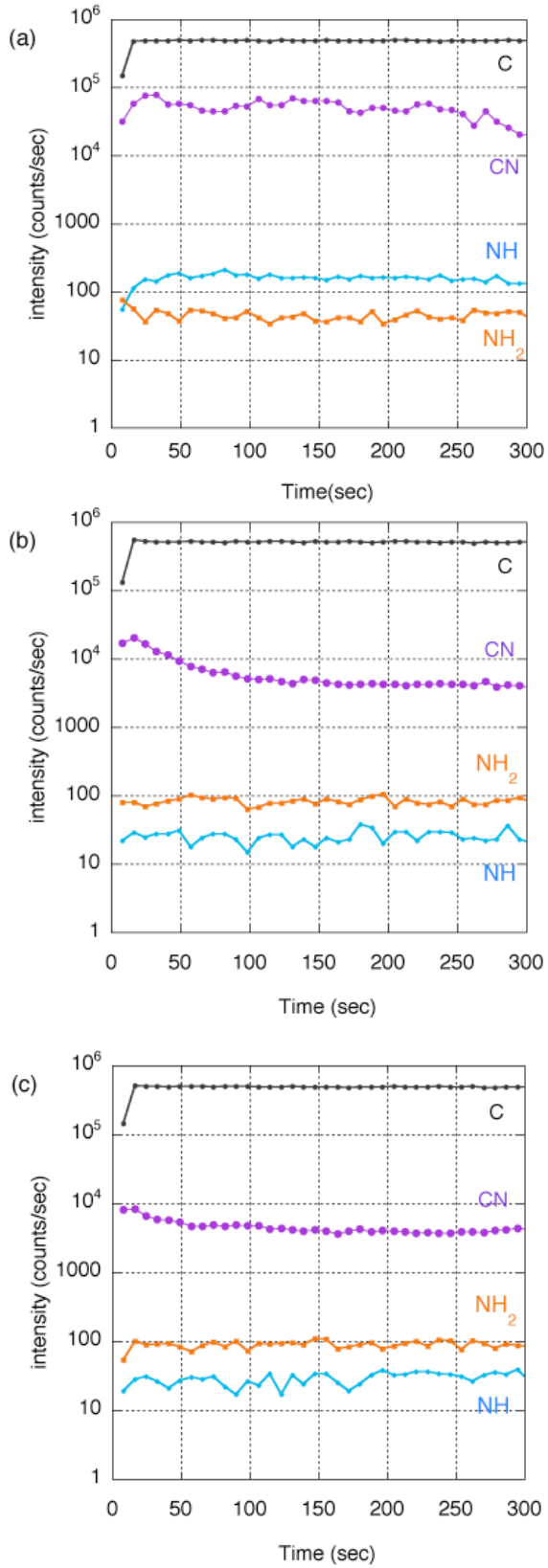

Figure 3.3.6. TOF-SIMS spectra of (a) the reference sample doped with urea, (b) the sample doped with DMU 1000 ppm, and (c) the sample doped with DMU 10 ppm [7].

As a summary, synthesis of N-doped diamond thin film was conducted, and field emission properties of the obtained films were investigated along with their C-N concentration. Nitrogen incorporation was confirmed by TOF-SIMS, however, M-I-V type low-threshold field emission was not confirmed for the present samples.

Since a-Se based photodetectors do not require high-energy electron for their operation, it is preferable to use a cold cathode with low operation voltage: low operation voltage leads to low energy electron beam, which, less likely to cause recrystallization of a-Se by electron beam irradiation. It is also necessary to develop an emitter array in order to use the photodetector in imaging applications. To achieve this goal, fabrication of heavily N-doped diamond with extremely high resistivity is essential, since electron emission from flat surface should lead to small dispersion angle and thus high spatial resolution. The high resistivity may also be effective for simple fabrication process, since extraction grid can directly be deposited on the diamond surface without forming insulation layer.

References

[1] K. Okano, S. Koizumi, S. R. P. Silva, and G. A. J. Amaratunga, "Low-threshold cold cathodes made of nitrogen-doped chemical-vapour-deposited diamond," Nature 381,140 (1996)

[2] T. Inuzuka, "Diamond Thin Films," J. Surface Sci. Soc. Jpn (1990)

[3] Y. Kudo, Y. Sato, T. Masuzawa, T. Yamada, I. Saito, T. Yoshino, W. J. Chun, S. Yamasaki, and K. Okano, “Field emission from N-doped diamond doped with dimethylurea,” J. Vac. Sci. Technol. B 28, pp.506-510 (2010)

[4] M.J. Fransen, J. te Nijenhuis, J.H.A. Vasterink, R.L Stolk, and J.J. Schermer, "Analysis of the Surface Morphology of CVD-grown Diamond Films with X-ray Diffraction," Advances in X-ray Analysis 46, pp185-191 (2003)

[5] American Society of Testing Materials, 6-0675

[6] S. A. Solin and A. K. Ramdas, "Raman Spectrum of Diamond," Phys. Rev. B 1, 1687–1698 (1970)

[7] T. Masuzawa, Y. Sato, Y. Kudo, I. Saito, T. Yamada, A. T. T. Koh, D. H. C. Chua, T. Yoshino, W. J. Chun, S. Yamasaki and K. Okano, "Correlation between low threshold emission and C–N bond in nitrogen-doped diamond films," J. Vac. Sci. Technol. B 29, 02B119 (2011)

[8] R. H. Fowler and L. Nordheim, “Electron Emission in Intense Electric Fields,” Proc. R. Soc. London, Ser. A 119, 173 (1928)

[9] P. Dyke and W. W. Dolan, “Field Emission - Advances in Electronics and Electron Physics,” 8, Academic Press, New York (1956)

[10] Y. Kudo, T. Yamada, H. Yamaguchi, T. Masuzawa, I. Saito, S. Shikata, C. E. Nebel, and K. Okano, “Field Emission from Modified P-Doped Diamond Surfaces with Different Barrier Heights,” Jpn. J. Appl. Phys. 47, 8921 (2008)

[11] T. Yamada, A. Sawabe, S. Koizumi, J. Itoh, and K. Okano, “Potential profile between boron-doped diamond electron emitter and anode electrode,” Appl. Phys. Lett. 76, 1297 (2000)

[12] K. Okano, T. Yamada, A. Sawabe, S. Koizumi, J. Itoh, and G. A. J. Amaratunga, “Metal-insulator-vacuum type electron emission from N-containing chemical vapor deposited diamond,” Appl. Phys. Lett. 79, 275 (2001)

Chapter 4. High sensitivity photo detection utilizing carrier multiplication

As described in Chapter 1, a-Se based photodetector was successfully driven by diamond cold cathode. In addition, the a-Se target has been optimized for better stability, of which detail is presented in Chapter 2. The next step is to demonstrate the high-sensitivity photo detection utilizing carrier multiplication, as well as investigate the fundamental conditions to induce this carrier multiplication. Understanding the mechanism of carrier multiplication is not only useful to utilize this effect in diamond-driven device, but also to extend high-sensitivity photo detection to the wavelength beyond visible range, i.e. ultraviolet and X-ray. Toward this end, high-sensitivity photo detection utilizing carrier multiplication has been attempted in this chapter. The optimized a-Se films are deposited and stabilized using the procedure presented in Chapter 2, and contact current *versus* applied voltage (I_C-V) characteristics are measured to confirm carrier multiplication in the a-Se films. The films are then combined with N-doped diamond cathode to fabricate prototype diode-structured photodetectors, of which sensitivity is characterized by emission current *versus* applied voltage (I_{em}-V) measurement. The sensitivity is evaluated in terms of nominal quantum efficiency.

4.1. Clarification of remaining issues in the prototype photodetector [1]

In order to optimize a photodetector that consists of a-Se target and N-doped diamond cathode, it was necessary to clarify remaining issues in this device. For this

purpose, sensitivity to visible light was evaluated using the prototype photodetector. I_{em}-V characteristics and photo response were taken under illumination of red (R), green (G) and blue (B) light to confirm the sensitivity to each of the light [1].

Figure 4.1.1 illustrates the diode-structure photodetector used in this measurement. This device is essentially same as the one presented in the literature [2-4]. It consisted of two components: an a-Se based photoconductive target was used as the anode, and N-doped polycrystalline diamond thin-film was used as the cathode.

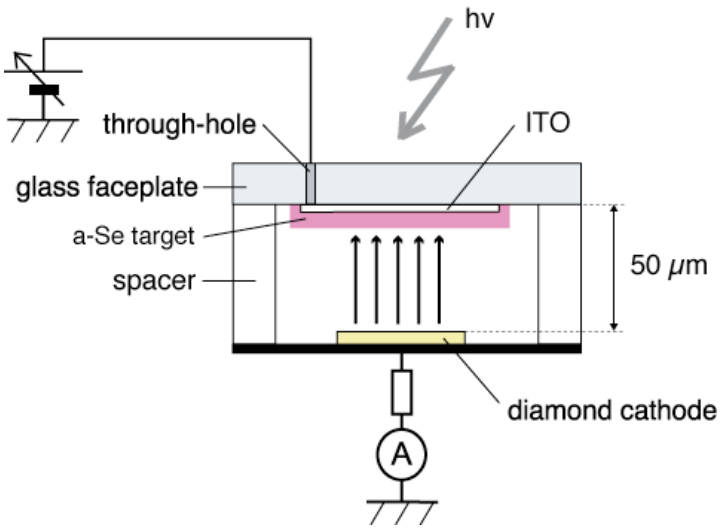

Figure 4.1.1. Schematic diagram of diode-structure photodetector consisting of a-Se based photoconductive anode and N-doped diamond cathode [1].

The a-Se based anode was deposited by vacuum evaporation. Three types of evaporation source were used for the deposition: Se, As_2Se_3 and Te grains were filled in separate molybdenum boats, and glass substrates fixed on a turntable rotated over each of the evaporation source to form a multi-layered film. A glass faceplate equipped with conductive through-hole was used as the substrate, on which indium-tin-oxide (ITO) thin-film was deposited by sputtering that served as transparent contact. The detailed deposition setup was described in the literature [5].

The N-doped diamond thin-film was obtained by hot filament CVD, of which setup was presented in Chapter 3. The deposition conditions were as follows. The filament temperature monitored by a pyrometer was 2,300 ^{o}C, substrate temperature measured by thermocouple was ~ 850 ^{o}C, reaction pressure was 100 Torr, and the ratio of the reactant gas to hydrogen was 0.6 vol. %. Urea was used as N-source, which was first dissolved by methanol to form a saturated solution and then diluted to 1/10 by acetone. The diamond thin-film was grown on n-type Si (100) surface for 2 hours to form polycrystalline diamond film with 8 μm thick.

The anode and the cathode were then combined into a diode-structure photodetector. The distance between the anode and the cathode was kept at 50 μm using Teflon spacer. The entire setup was mounted in a fixture made by Macole, and introduced in a vacuum chamber to be evacuated to 10^{-8} Torr. The measurement was conducted as follows. A positive bias of up to 2,000 V was applied on the anode, which induces field emission from the cathode. The emission current (I_{em}) was measured by an ammeter connected to the cathode side of the detector, and plotted as a function of the applied voltage (V). This I_{em}-V measurement was conducted under different lighting conditions. The entire measurement system was carefully designed so that leak current is lower than 0.1 nA, which was the detection limit of R6441C ammeter.

Figure 4.1.2 shows typical I_{em}-V characteristics of the detector when illuminated by white halogen light. Each line represents I_{em}-V characteristic under a fixed intensity of light. The result showed that the incident light induced the increase in the emission current, proving successful photodetection [1]. The change in the emission current by light illumination was defined as the photo-response. The photo-response occurred for light intensities as low as below 0.39 lx. This low illuminance of 0.39 lx was approximately the same to the brightness under moonlight, where clear image cannot be taken by using

normal silicon based devices such as CCDs or CMOS sensors unless it was cooled down by Peltier device or liquid nitrogen to eliminate thermal noise [1].

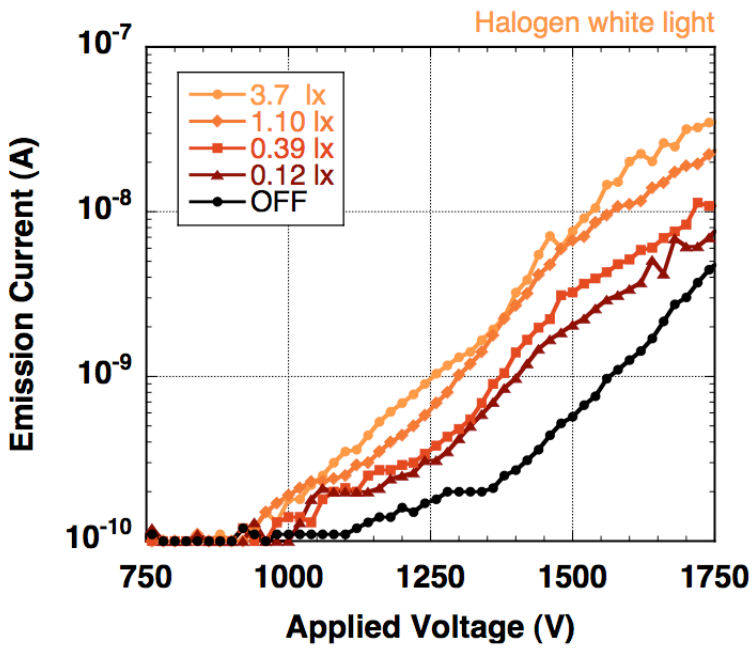

Figure 4.1.2. I_{em}-V characteristics of a-Se based photodetector under different lighting conditions [1].

The same I_{em}–V measurements were then conducted for different wavelengths: red, green and blue (RGB) filtered light were used to illuminate the detector, each under the same manner. Measuring photo-response towards three primary colors of light was obviously essential for future applications and practical usage as camera tube. Figures 4.1.3(a)–(c) are the I_{em}–V characteristics under RGB lights, respectively. The peak position for each color was at 1.85 eV (670 nm), 2.17 eV (570 nm), and 2.38 eV (520 nm), respectively. Since a-Se was reported to have an optical band gap of 2.0 eV and could not detect red light [6], this a-Se film was modified by tellurium (Te) doping. Doping Te was known to narrow the band gap of a-Se down to 1.8 eV, which enabled photoconductive film to detect red light [6]. The emission current corresponding to the red light was almost equivalent to the emission current measured under green or blue light for the same illuminance. This result showed that Te

intensified the photo-response towards red light when it was successfully doped into a-Se, where a-Se without doping Te could not detect red light illumination.

Although these I_{em}–V characteristics proved a successful photo detection, a few issues were found in the current photodetector. Figure 4.1.2 suggested that the operation voltage of this photodetector was at least 1000 V and could potentially reach 2000 V. This voltage was necessary to induce electron emission from the cold cathode. Such a high operation voltage not only required large insulating buffer and bulky voltage source, but also might lead to degradation of a-Se film due to crystallization caused by high-energy electron beam. The degradation of a-Se film was in fact observed in some of these experiments, which led to diminishing photocurrent after continuous operation.

A possible solution to this is stabilization of a-Se film by changing its elemental composition. Increasing As incorporation can increase the stability of a-Se, although it leads to lower photocurrent. Another approach is to decrease the operation voltage of the cold cathode, either by reducing the anode-cathode distance or by using cold cathode with lower extraction voltage. Reducing the operation voltage of the cold cathode lowers the energy of electron beam, and prevent crystallization induced by e-beam bombardment. Lowering the energy of electron beam is also effective to reduce thermal stimulation to the a-Se target, since the Joule heat is limited by a product of energy and current of electron beam.

Another issue to note was that the dynamic range of the detector was limited: although the photocurrent was up to one order of magnitude higher than the dark current in all cases, the difference between photocurrent under different illumination was not distinctive in Figure 4.1.3 (a) and (b). This should be due to the limited number of photo-induced carriers. Applying carrier multiplication effect to this device should drastically increase the number of generated carriers, and should improve the dynamic range at low illuminances.

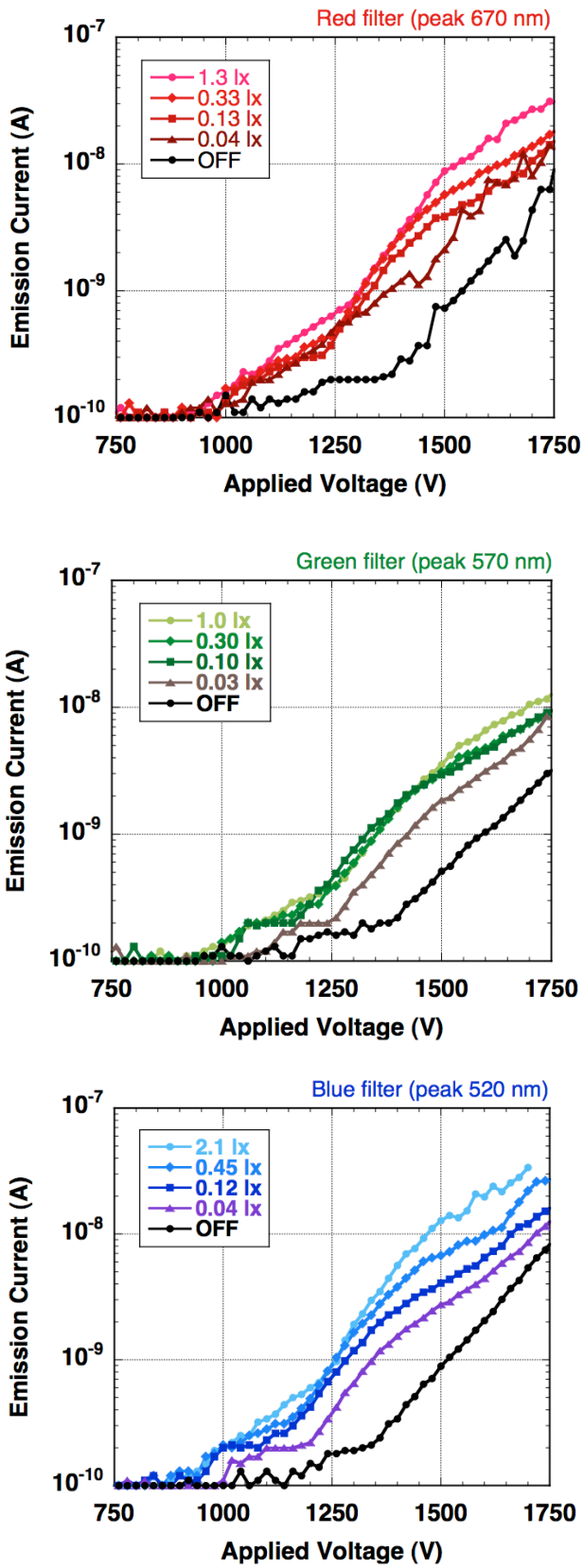

Figure 4.1.3. I-V characteristics of a-Se based photodetector illuminated using different color filters: (**a**) red with peak wavelength 670 nm, (**b**) green with peak wavelength 570 nm and (**c**) blue with peak wavelength 520 nm [1].

Following the I_{em} -V measurement, the photo response was further investigated by the emission current *versus* operating time (I_{em} -T) under RGB light using the same measurement setup. Figure 4.1.4 (a)–(c) shows the I_{em}-T characteristics measured under RGB, respectively. The anode voltage was fixed at 1,500 V, and the RGB illumination was given in 10 mHz pulse. The results showed a similar result observed in the I_{em}-V characteristics where an increase of the emission current was observed even for the low illumination of 0.1 lx. When the illuminance was higher, the difference between the dark current and the photocurrent became larger. However, the photo-response was slightly slow, which was caused by the transient surface potential of a-Se based film due to the diode structure [3]. Triode structure, which could control the extraction voltage independently from the anode voltage, was expected to improve slow response [7]. It should also be noted that the signal to noise (S/N) ratio decreased as the illuminance was decreased, due to the limited number of photo-generated carriers.

To summarize the discussion above, the sensitivity to RGB light was characterized using a prototype photodetector. I_{em}-V characteristics and I_{em}-T characteristics showed a successful photodetection even under the low illuminance of 0.1 lx, however, following issues were found. Firstly, the a-Se film degraded by crystallization due to the high operation voltage. A cold cathode used for signal read-out should be redesigned for better stability and lower operation voltage to avoid hi-energy electron bombardment. The stability of a-Se target should also be increased. Secondly, the photocurrent was limited and S/N ratio was low at low illuminance, due to the limited number of photo-generated carriers. By applying carrier multiplication effect, the number of carriers should be greatly increased, and should lead to high S/N ratio even at low illuminances. The improvement in a-Se target and cold cathode are discussed in the next section.

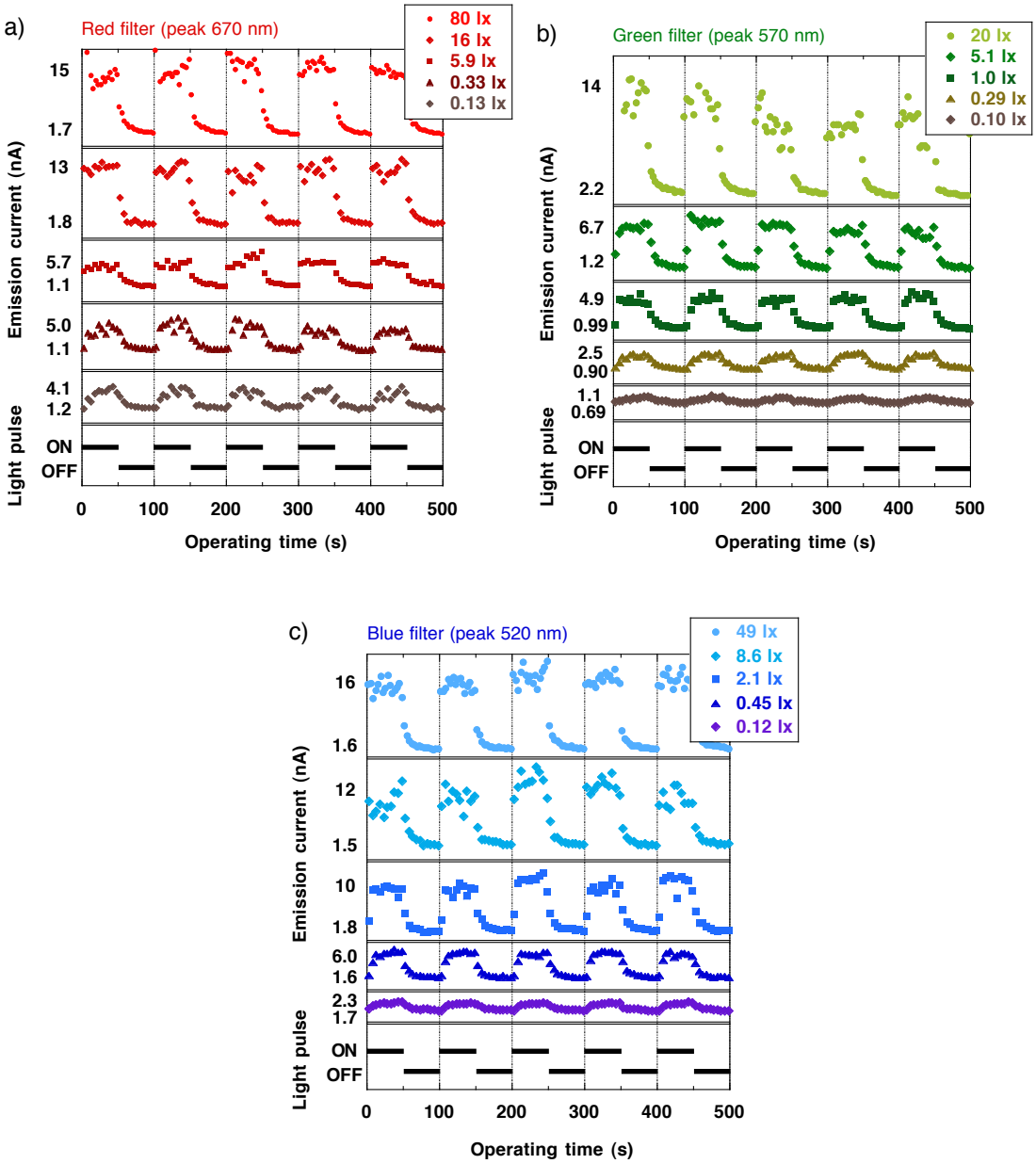

Figure 4.1.4. I-T characteristics of a-Se based photodetector illuminated with filtered halogen lamp [1]. Peak wavelengths of the lights were (**a**) 670 nm for red filter, (**b**) 570 nm for green and (**c**) 520 nm for blue.

4.2. Preparation of optimized a-Se films and their I_C-V characteristics

As presented in the last section, it was necessary to optimized a-Se target in order to increase its stability and enables carrier multiplication. To this end, optimization of a-Se film has been investigated. As mentioned in the previous section, a-Se can shift into crystalline selenium or another quasi-stable state, by stimulations such as annealing, light irradiation and e-beam irradiation. It was also mentioned in Section 2.2.1 that As incorporation is an effective way to prevent anneal-induced degradation of a-Se film.

In this section, a-Se films are deposited with small amount of As incorporated through the rotational evaporation. The structure of the films is then characterized using secondary ion mass spectroscopy and Raman spectroscopy to confirm the stabilization effect. The optimized a-Se films are then characterized by contact current *versus* applied voltage (I_C-V) measurement to demonstrate carrier multiplication effect.

The selenium-based amorphous films are deposited by vacuum evaporation, using the stabilization procedure presented in Chapter 2. Trigonal selenium (t-Se) pellets are used as the evaporation source, whereas small amount of arsenic is incorporated by evaporating As_2Se_3 to prevent thermal degradation of the films [8] As described in Chapter 2, incorporation of As increases the stability of a-Se film but reduce its photocurrent. The amount of As incorporation was optimized for maximum photocurrent while maintaining its stability. The multi-layered films are deposited on substrates that consist of a glass faceplate with a carbon through-hole and indium-tin-oxide (ITO) thin film serving as a transparent contact. The films are then annealed on a hot plate, at temperatures between 45 ºC to 65 ºC in 5 ºC step for a total of 25 min. The annealing temperature is carefully selected so that the films does not crystallize by the heat. The annealing was conducted under the atmospheric pressure.

The depth profile of the film composition is characterized using time-of-flight secondary ion mass spectroscopy (TOF-SIMS) in order to confirm the multilayer structure of As-incorporated a-Se film [9]. In the TOF-SIMS measurement, the surface of the film is alternately bombarded by ion beams for etching and analysis, which enables one to take a depth profile of the composition. The measurement is conducted using ION-TOF, TOF.SIMS5 system, under the following conditions: Ga, and Cs ion beams are used to analyze and sputter etch the sample, respectively. The Ga ion gun is operated at an acceleration voltage of 25 kV and the beam current of 1.5 pA. The Cs sputter beam is operated at acceleration voltage of 1 kV and beam current of 4 nA. The spot size of the analysis beam is set to 100 μm × 100 μm and the sputtered area is 200 μm × 200 μm. Both analysis beam and sputter etching beam are alternately irradiated for 4 s. Since this measurement is destructive, the analysis area is marked and avoided for further analysis.

A typical TOF-SIMS spectra of the film, focusing on ^{78}Se, ^{80}Se, and ^{75}As, are illustrated in Figure 4.2.1 (a). Both Se and As signals showed oscillating peaks, whose number matched the number of times the film swept over each of the evaporation boats during the film deposition. The thickness of each layer was calculated from the etching rate, and was estimated to be 15 nm. Since the film consisted of Se layers and As-rich Se layers, there should be a phase shift between Se and As signals. However, the shift was less visible due to the angle of the sputtering beam allowing the alternative layer to etch away on its way, which led to the modulation in the signal. From the TOF-SIMS spectra, it is evident that the films have multi-layered structure with different arsenic content, as shown in Figure 4.2.1 (b). A quantitative analysis of arsenic concentration is difficult at present, due to the lack of reference samples.

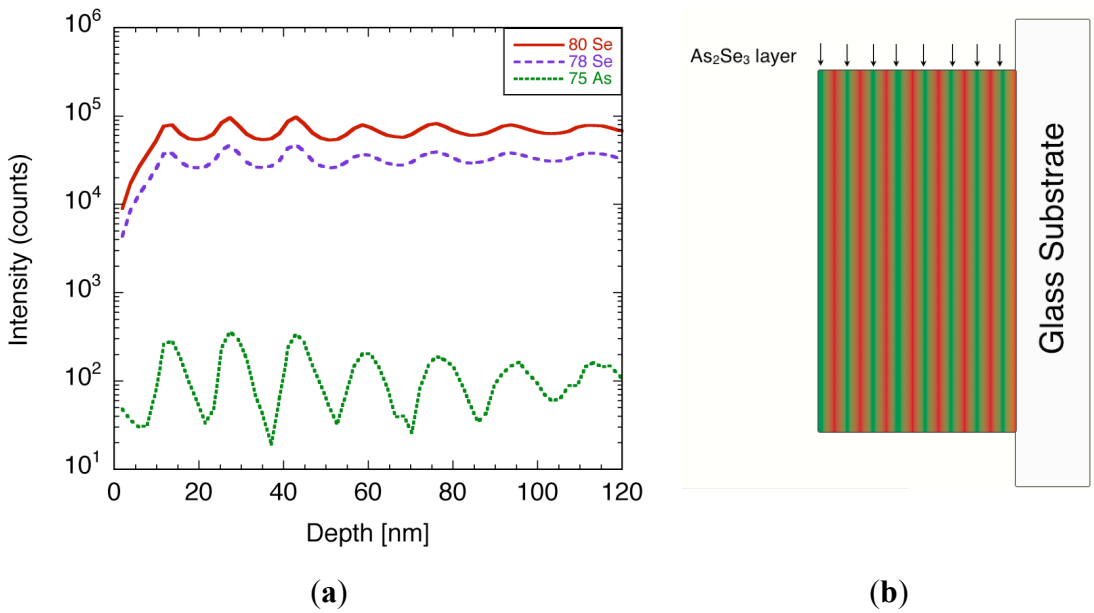

Figure 4.2.1. (**a**) Typical TOF-SIMS spectrum of As-incorporated a-Se film. (**b**) Schematic diagram explaining the structure of the deposited film using Se and As_2Se_3 as evaporation source [9].

In order to evaluate the stability of As-incorporated a-Se, the structures of the films were characterized using Raman spectroscopy. It was reported in the previous studies that a-Se recrystallized into t-Se by laser illumination in Raman spectroscopy system [9], in addition to the thermally induced transition mentioned above.

The a-Se films with different As content were measured by Raman spectroscopy, and changes in the spectra were compared for different signal accumulations. The measurement system used in this study was triple monochrometer Raman system (Dilor XY800) equipped with a CCD camera for multi-channel detection. The deposited films were placed in an ultra high vacuum chamber, and were illuminated by an excitation laser, which was the 1.92 eV (647.1 nm) emission line of a Kr ion laser. The monochrometer slits were set for a resolution of 2.4 cm^{-1}. The laser with a power of 18 mW was focused to a spot of approximately 200 μm in diameter on the sample surface. All Raman spectra

were recorded in a backscattering geometry. A detailed description of this setup was given in [10].

Figure 4.2.2 illustrates the Raman spectra for the film with and without As incorporation [4]. The relatively broad feature with a peak at 250 cm^{-1} was characteristic to a-Se, and the sharp peak at 235 cm^{-1} represented t-Se, which was produced by crystallization [11]. The results shown in Figure 4.2.2 demonstrated that the a-Se peak in the As-incorporated film remained even after 50 accumulations. In contrast, Raman spectrum for the pure a-Se film showed that the a-Se peak decreased rapidly after 9 accumulations and almost disappeared after 50 accumulations. The crystalline t-Se peak appeared at 233 cm^{-1} and dominated the spectrum after 50 accumulations, meaning that the film had almost entirely crystallized into t-Se.

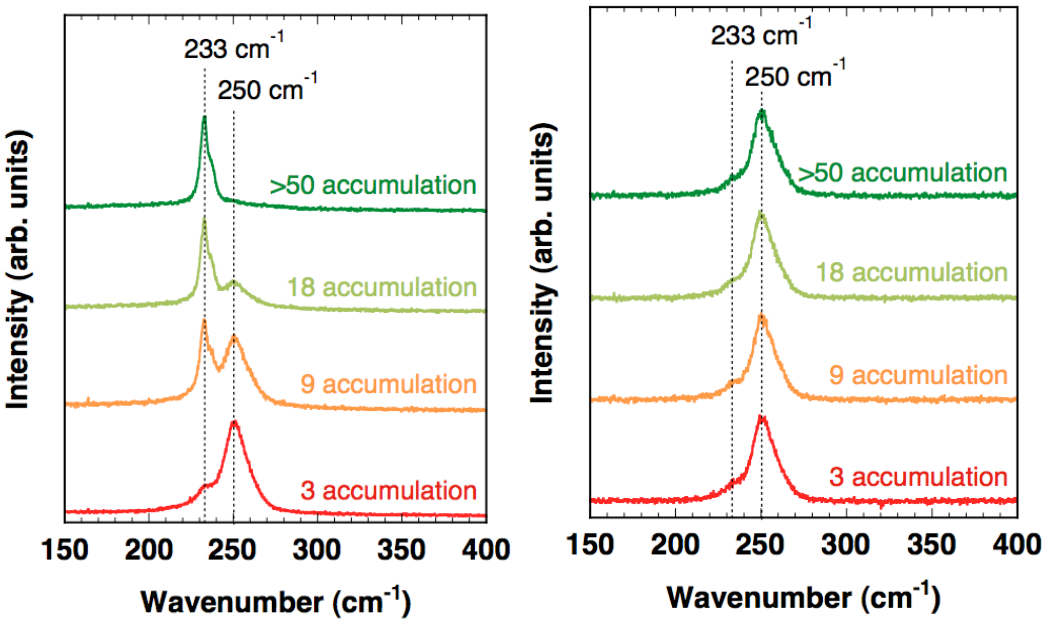

Figure 4.2.2. Raman spectra of the deposited film: (**a**) without As incorporation and (**b**) with As incorporation [9,11].

Raman spectrum showed that amorphous structure is maintained for the multi-layered film, whereas a-Se films without As_2Se_3 layers crystallized under laser

exposure during the measurement. The resistivity of the crystallized films was typically lower by orders of magnitude than that of amorphous films, so that it is difficult to induce intense electric field in such crystallized films. Since the carrier multiplication requires application of an electric field of 80~100 V/μm across the film [12-14], the high resistivity of amorphous film must be maintained by As doping.

Once the film composition and the structure are confirmed, the electronic properties of the multi-layered films are evaluated by contact current versus applied voltage (I_C-V) measurements using the setup depicted in Figure 4.2.3.

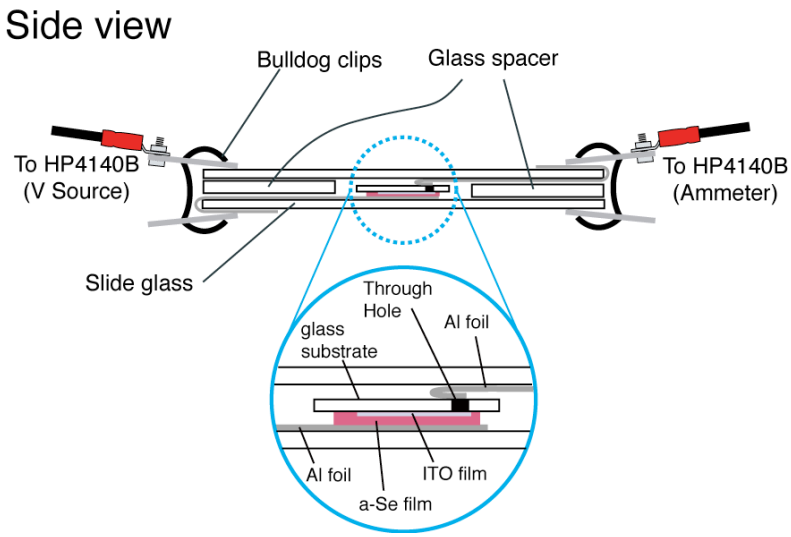

Figure 4.2.3. Schematic diagram of the experimental setup used for I_C-V measurement. [8].

The measurement is conducted under illuminance of 2,000 lx using white halogen lamp. A typical I_C-V characteristic of the film is presented in Figure 4.2.4. The contact current (I_C) shows a linear increase as the applied voltage increases from 0 V, but shows a drastic current increase at voltage above 340 V. This transition of the I_C-V curves is reproducible for each iterative measurement on the same sample, thus it is apparent that the sample has not been irreversibly destroyed. One may note that neither carrier blocking layers nor any contact insulator are introduced to cause the carrier multiplication, despite

the previous reports[12-14].

In contrast to the As-incorporated films, the transition in I_C-V characteristic is not observed in a-Se film without As incorporation. The contact current was larger by up to two orders of magnitude for pure a-Se films, and high voltage could not be applied due to the current limit. These films were possibly crystallized in the first few measurements, and ended up having a resistivity lower by orders of magnitude than that of amorphous films. Such a low-resistive film was not suitable for high-sensitivity photo detection: the carrier multiplication was reported to take place under strong electric field of 80~100 V/μm [12-14], and a high-resistivity was essential to maintain this strong electric field. The Raman spectra clearly showed that the As-incorporated multilayer film was effective to maintain high resistive amorphous structure that was suitable for the carrier multiplication.

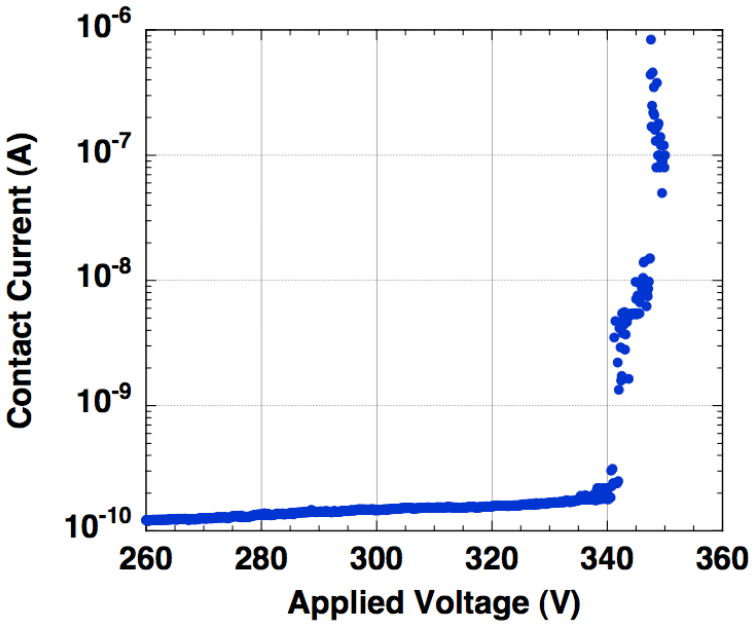

Figure 4.2.4. A typical I_C-V characteristic of an optimized a-Se film [9].

In order to explain the exponential current increase in I_C-V characteristics, a multi-layered structure of the films should be considered. It is well known from previous

reports that, a-Se contains high defect density, so that it can be regarded as an intrinsic semiconductor with many carrier traps [15]. Assuming a contact area of 2 cm^2, the resistivity of the film is estimated to be over 1.6 x 10^{16} Ωcm, using I_C-V curve at voltage lower than 340 V. The extremely high resistivity of the film is attributed to low carrier concentration due to high trap density [16]. It is also known that a-Se shows weak p-type conduction by arsenic incorporation [16]. Therefore, the structure of the obtained films is assumed to be the alternative trapping layers (a-Se) and p-type layers (a-Se:As).

The carrier multiplication in the multi-layered films can be described by following steps:

1) Primary carrier pairs are generated by incident light
2) The carriers are accelerated in the a-Se:As layer, because of the intense electric field in the film
3) The accelerated carriers enter the a-Se layer, which excite multiple carriers from the traps
4) The excited carriers enter the a-Se:As layer, in which they are accelerated for the next carrier cascade

An advantage of this "cascading multiplication" is that it can reduce the dark current even in signal multiplication mode. Since little or no incident photon is expected in the dark, most carriers are trapped in the trapping layer. This prevents carriers to enter the p-type layer, where they are accelerated enough to cause carrier multiplication.

The average electric field required for the carrier multiplication is calculated to be 170 V/μm, which is approximately two times larger than previous reports. The electric field to induce carrier multiplication is 80 V/μm in the literature [12-14]. It is assumed that this difference is because of the multilayer structure of the film: either one of the doped or non-doped layers, or the boundary of the two layers contribute to dark current reduction,

rather than carrier multiplication. A detailed analysis on the layer design and electronic properties for optimum multiplication/low dark current balance is currently under investigation.

4.3. Device operation for the high-sensitivity photo detection

One of the key issues in the current photodetector found in Chapter 4.1 was degradation of a-Se target. The cause of this degradation was both structural instability in a-Se target and high-energy electron beam used as signal read-out. As the stability of a-Se target has been optimized in the previous section, next step is to examine the signal read-out system. In this section, the structure of the photodetector, as well as N-doped diamond cold cathode, has been redesigned.

First of all, the operation voltage of the photodetector is reconsidered. In a diode-structure photodetector, the operation voltage determines the energy of electrons that are used for signal read-out. Since the irradiation of high-energy electron beam can degrade a-Se target, the energy of the emitted electrons should be as small as possible. In order to reduce the energy of emitted electrons, the extraction voltage of the cold cathode, or the voltage where emission current starts to flow, was characterized by I_{em}-V measurement. In the discussion below, the extraction voltage is defined as the voltage where emission current of 1 nA is obtained.

The I_{em}-V characteristics of cold cathodes, the one used in the existing photodetector and the one optimized in this study, are shown in Figure 4.3.1. The extraction voltage of the previous cold cathode was approximately 1,300 V, while the optimized emitter had extraction voltage of around 550 V. In the diode-structured photodetector, the extraction voltage can be controlled by the anode-cathode distance. Other factors that determine the extraction voltage are various parameters in the cold

cathode, such as surface morphology, surface termination, thickness of the diamond film, as well as nitrogen concentration [17,18]. In this study, the anode-cathode distance and the emitter were optimized so that its extraction voltage is as close as the voltage required for the carrier multiplication. The reason to this is as follows.

Since the carrier multiplication occurs under intense electric field of 80-100 V/μm, the high electric field must be built up in the a-Se film. This high electric field cannot be built up if external carriers are injected into a-Se either from electrical contact or electron beam from the cathode. For this reason, injection of external carrier needs to be prevented [12,19]. Previous studies reported that fabricating blocking layer on a-Se film is necessary to prevent carrier injection and to build up the electric field for carrier multiplication [19,20]. In these studies, hot cathode was used as signal read-out, where electrons were "pushed towards the film" and carrier injection occurs naturally.

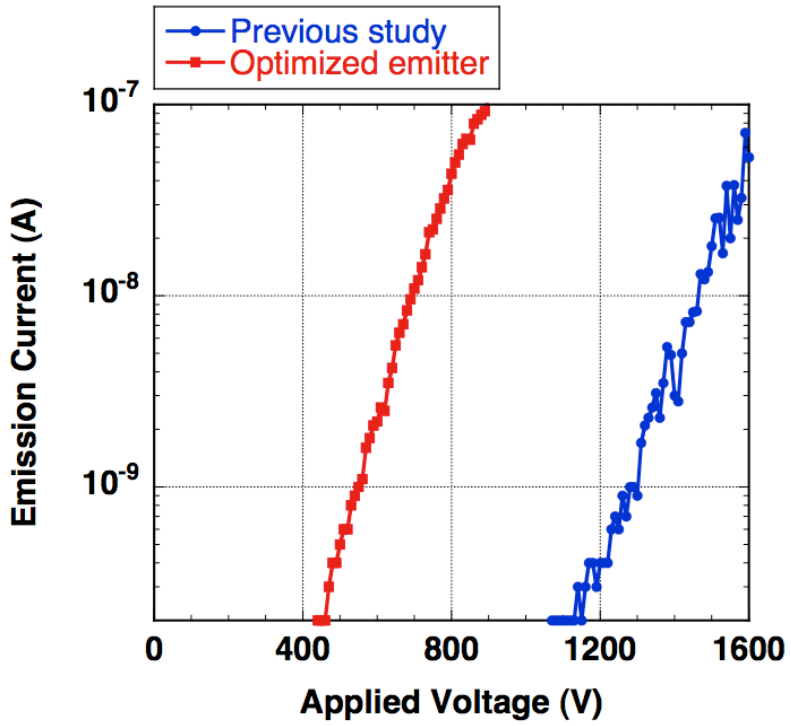

Figure 4.3.1. I_{em}-V characteristics of N-doped diamond cold cathodes. The optimized emitter was chosen so that its extraction voltage was almost same as the voltage required to induce carrier multiplication.

In this study, however, alternative method has been proposed, which can only be used for a diode-structure device driven by a cold cathode. In cold cathode, electrons are extracted by the potential difference between a-Se and the cold cathode. In other word, the electron beam is "pulled by the film". Therefore, by choosing the proper cold cathode, one can prevent carrier injection without having blocking layer on the a-Se target. The emission current starts to flow *after* the electric field has built up. This new method also determines the minimum extraction voltage. If we choose a cold cathode with extraction voltage much lower than the voltage required for the carrier multiplication, the emission current starts to flow before the carrier multiplication starts. This would induce electron injection into the a-Se film and prevent the electric field from building up. Therefore, the extraction voltage of the cold cathode should be optimum so that it is as low as possible to reduce the damage to a-Se, while is higher than the voltage to induce carrier multiplication.

Another improvement in the optimized photodetector is its operation procedure. During the I_{em}-V measurement for Section 4.1, it was found that a-Se target degrades on the first measurement attempt: the I_{em}-V characteristics of the first run and the one taken in the following attempts are presented in Figure 4.3.2. In the first run, the emission current was not observed until 1,100 V, after which the current rapidly increased up to as large as 0.1 mA, which is well beyond the safety limit of our experimental setup. Despite its unstable emission characteristic on the first run, the emission current became much more stable and the extraction voltage was decreased down to ~ 300 V.

The characteristic I_{em}-V curve of the first run could be explained by removal of adsorbate from the cathode surface. Since the surface adsorption greatly modifies the

potential barrier at a surface, any adsorbates such as water or cleaning agent can prevent field emission. With such adsorption, the field emission occurs at relatively high voltage. Once the emission starts, this adsorbate is removed from the surface due to the emission current and the Joule heat, which leads to rapid increase in emission current. The removal of surface adsorption, or the "flushing" process, is commonly used in devices using cold cathode. In the present device, however, this flushing process degrades the a-Se target due to the high-energy electron bombardment.

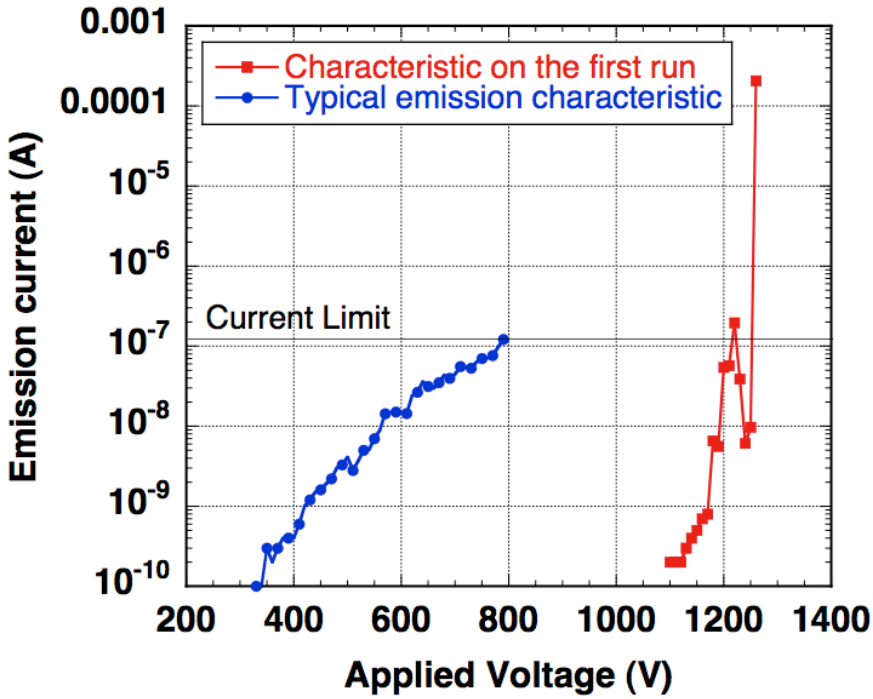

Figure 4.3.2. I_{em}-V characteristics of a diode-structure photodetector. The emission current showed a rapid increase in the first run, where surface adsorbate was flushed away. The emission characteristics after the first run showed much more stable increase, and had lower extraction voltage.

In order to minimize the degradation of a-Se through flushing process, an insulating nature of a-Se anode has been focused. In the previous studies, the flushing process was conducted without light illumination. In this case, the a-Se film behaved as

insulator, and no carriers were expected neither inside nor the surface of the film. As a result, the surface of a-Se had floating potential. This might have prevented the field emission to occur, since the field emission depends on the electric field at the cathode surface, which is determined by the surface potential of a-Se and the cathode.

Based on this hypothesis, the flushing process was carried out under the illuminance of 3,5000 lx using halogen lamp. This light illumination should increase the conductivity of a-Se, which reduces the voltage where electron emission starts. By using this method, the field emission occurred at around 500 V, which was only slightly higher than the typical extraction voltage of the cathode. After 10 iterative measurements, the extraction voltage gradually decreased, and the I_{em}-V characteristics came to the same as typical one.

As discussed above, the flushing process of the cold cathode has found to be a key factor in the degradation of a-Se target. By illuminating the a-Se target with high illuminance of ~ 3,500 lx, the cathode was successfully flushed without causing noticeable damage to a-Se target. Another solution is to introduce a mesh grid above the cold cathode and use it for flushing process. This flushing process should be useful for a triode-structure photodetector, which is presented in Chapter 1.

As a summary, optimization of signal read-out system has been attempted in this section by choosing N-doped diamond having extraction voltage close to the voltage required to induced carrier multiplication. The flushing process of this cold cathode was also examined, which resulted in an optimized flushing procedure. The next step is to apply these techniques to demonstrate the high-sensitivity photo detection.

4.4. High-sensitivity photo detection utilizing carrier multiplication

Now that the a-Se target has been optimized and the operation procedure

redesigned, the prototype photodetector is assembled and high-sensitivity photodetection is investigated.

The a-Se target, which is optimized in the process presented in section 4.2, is mounted as a photoconductive anode in a photodetector in order to apply carrier multiplication to high-sensitive photo detection. The structure of the prototype photodetector is schematically depicted in Figure 4.4.1.

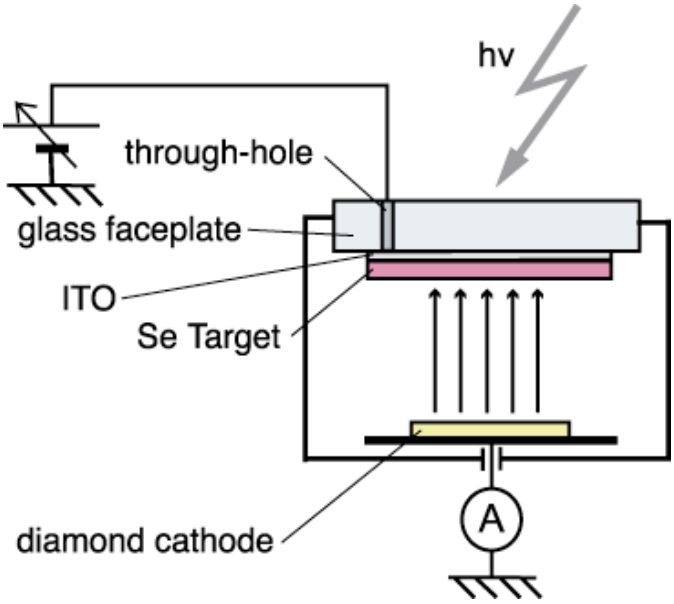

Figure 4.4.1. Schematic diagram of a diode-structured photodetector [1].

This diode-structured detector consists of two parts: a-Se based photoconductive film on anode side and diamond electron emitter for signal readout. The anode and the cathode are fixed in a ceramic jig, with their distance kept at 100 μm using a Teflon spacer. The setup was introduced in a vacuum chamber with a base pressure of 10^{-8} Torr, and electron emission was induced by applying voltage between the anode and the cathode. HP 4140B was used as a voltage source, whose output was intensified 1,000-fold using a Glassman high voltage DC power supply. The emission current was measured by an Advantest R6441C digital multi-meter with a detection limit of 0.1 nA. A white halogen

lamp with 38,000 lx (Kenko, KTS-50RSV) is used to illuminate the detector. A nitrogen (N)-doped diamond film with threshold voltage at around 400 V is specifically chosen as a cathode, in order to apply high voltage of up to 340 V across a-Se film to induce carrier multiplication.

Figure 4.4.2 shows a typical emission current *versus* applied voltage (I_{em}-V) characteristics of the photodetector. A signal to noise (S/N) ratio at voltage below 400 V is very high, due to low dark current of as low as detection limit (0.1 nA).

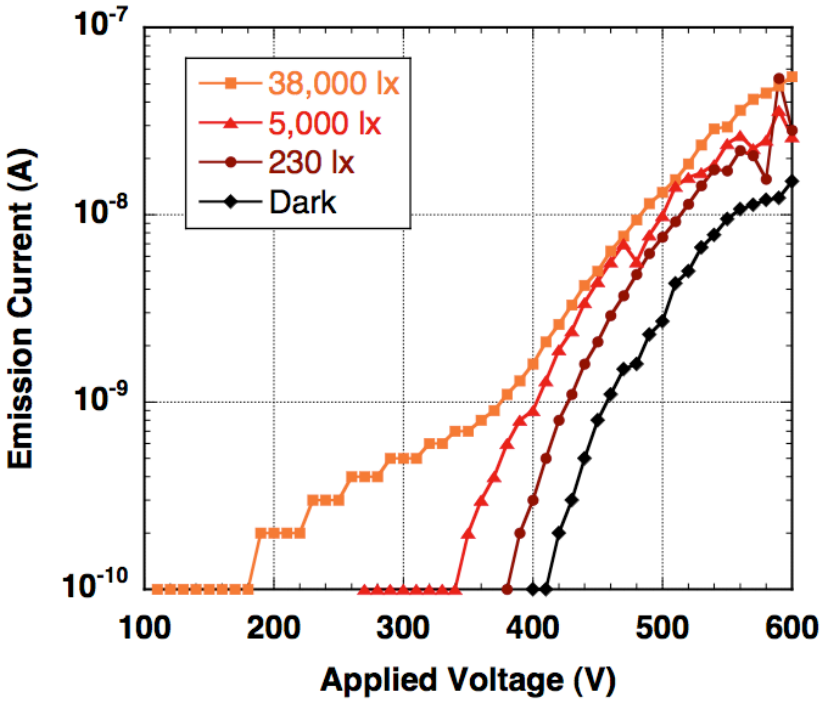

Figure 4.4.2. A typical I_{em}-V characteristic of the prototype diode-structure photodetector [9].

When the white light is turned on, the emission current is observed from 100 V, which is well below the threshold voltage of the emitter. The reason of this emission should be due to the hole accumulation at a-Se surface. Electron-hole pairs are excited by the light illumination, and positive holes accumulate on the cathode side of a-Se surface,

which increase the surface potential and thus enhance the electric field between the anode and the cathode. Previous study using diode-structured photodetector suggests that the potential of the film surface can modulate the electron emission from the emitter [3].

The emission current shows a steep rise at around 350 V under light illumination, however, the current increase is limited compared to the contact I_C-V characteristic (Figure 4.2.4). As the voltage increases, increase in emission current starts to diminish, and S/N ratio decreases. The cause of the diminishing current increase can be limited current supply from the emitter. Either high bulk resistance or carrier depletion in the emitter is suspected. A solution of this current limitation is introducing heavily N-doped diamond as electron emitter, which has M-I-V type electron emission. It is reported that in M-I-V type emission, the emission current is limited by electron injection between back contact and diamond film [17,18], which should prevent carrier depletion. The solutions to the current saturation, as well as improvement in S/N ratio at high current, remain as future tasks in order to achieve wide dynamic range.

The sensitivity of the photodetector is then estimated from the I_{em}-V characteristics. An increase in current density Δi in a photoconductor is usually expressed as follows:

$$\Delta i = e\mu\tau\eta N_0(1-\exp(-\alpha D))E \qquad (4.4.1)$$

where E is the electric field across the photoconductor, e is the elemental charge, μ and τ are the mobility and lifetime of the carriers, η is the quantum efficiency, N_0 is the number of incident photon, α is the absorption coefficient, and D is the thickness of the photoconductor. Reflection is assumed to be negligibly small in this study. The product $\mu\tau E$, or carrier Schubweg, is known to be a limitation factor when carrier path is long compared to the Schubweg. In this study, however, the thickness of the film is 2 μm, which is small enough to ignore the limitation from Schubwegs. Previous study reports

that the Schubweg of a-Se is 1.2 mm-12 mm for holes and 0.3 mm-1.2 mm for electrons [21]. The contribution of $\mu\tau E$ to the current is, therefore, assumed to be negligible.

Based on the assumptions above, nominal quantum efficiency, η_{nom}, is introduced to evaluate the sensitivity of the detector from measurable parameters. The definition of the nominal quantum efficiency is as follows:

$$\eta_{nom} = \frac{\Delta I}{eN_0(1-\exp(-\alpha D))} \qquad (4.4.2)$$

where, assuming that all the incident photons are absorbed within the photoconductor, the term $\exp(-\alpha D)$ becomes zero, so that one can estimate the nominal quantum efficiency from current and the number of incident photons.

In the emission current-applied voltage characteristic of the photodetector, 1 nA of current increase is observed at 400 V. The number of incident photons is roughly calculated assuming the wavelength of incident light to be 555 nm. The assumption is valid considering the mobility gap of a-Se, which is 2.2 eV without incorporation of tellurium [1,6]. Providing this condition, illuminance of the incident light is equivalent to 55.48 J/m^2s, which is 1.55 x 10^{20} photons per square meters per second. The area of the detection spot is estimated from the spot size of the emitter. It was reported that the emission area is smaller than 0.1 % of the emitter area [22], and is a few micrometer square in this study. Substituting these parameters to the equation (2), the nominal quantum efficiency of the present detector was calculated to be 10~40. This means that 10 to 40 carriers are created per incident photon, which is possible only if signal multiplication takes place. In the previous research it was reported that the HARP mode photodetector shows quantum efficiency of 10, which is in good agreement with the present results [12].

As a conclusion, conditions of the carrier multiplication in a-Se based films have been investigated by photoelectric measurements of the films with different configuration.

The conditions are

1) amorphous structure characterized by a broad Raman peak at 250 cm^{-1},

2) multi-layered film that consist of Se and As-rich Se layers,

3) contact current-applied voltage shows a rapid current increase at a certain voltage (340 V for a 2 μm thick film).

The nominal quantum efficiency calculated from the photo-detection experiments is 40, which is obviously enhanced by carrier multiplication. Further research on the signal multiplication mechanism should lead to a development of extremely high-sensitive photo imagers, which enable real-time imaging even with limited photon input.

References

[1] N. Kato, T. Masuzawa, Y. Kudo, Y. Kuwajima, H. Yamaguchi, K. Okano, T. Yamada, I. Saito, T. Butler, N.L. Rupesinghe and G.A.J. Amaratunga, "Sensitivity to red/green/blue illumination of amorphous selenium based photodetector driven by nitrogen (N)-Doped CVD diamond," Diam. Rel. Mater. 17, 95–99 (2008)

[2] Y. Suzuki, H. Yamaguchi, K. Oonuki, Y. Okamura, and K. Okano, "Amorphous Selenium Photodetector Driven by Diamond Cold Cathode," IEEE Electron Device Lett. 24, 16-18 (2003)

[3] K. Oonuki, Y. Suzuki, H. Yamaguchi, K. Okano, and Y. Okamura, "Diode structure amorphous selenium photodetector with nitrogen (N)-doped diamond cold cathode," J. Vac. Sci. Technol. B 21, 1586 (2003)

[4] N. Kato, I. Saito, H. Yamaguchi, H. Okamura, K. Okano, T. Yamada, T. Butler, N. L. Rupesinghe and G. A. J. Amaratunga, "Fabrication of an a-Se based photodetector driven by nitrogen-doped CVD diamond," J. Vac. Sci. Technol. B, 24, 1035 (2006)

[5] I. Saito, W. Miyazaki, M. Onishi, Y. Kudo, T. Masuzawa, T. Yamada, A.T.T. Koh, D.H.C. Chua, K. Soga, M. Overend, M. Aono, G.A.J. Amaratunga, and K. Okano, "A transparent ultraviolet triggered amorphous selenium p-n junction," Appl. Phys. Lett. 98, 152102 (2011)

[6] M. Kubota, "Progress in Development of HARP Imaging Device and Its Application," Journal of the Institute of Image Information and Television Engineers, Vol. 64, No. 3, 289-292(2010)

[7] Y. Suzuki, K. Oonuki, H. Yamaguchi, Y. Okamura, and K. Okano, "Triode-structure amorphous selenium photodetector driven by diamond cold cathode," Electron. Lett. 38, 25 (2002)

[8] I. Saito, K. Oonuki, T. Yamada, M. Aono, T. Butler, N. L. Rupesinghe, G. A. J. Amaratunga, W. I. Milne and K. Okano, "Anneal-Induced Degradation of Amorphous Selenium Characterized by Photoconductivity Measurements," Jpn. J. Appl. Phys. 44, L334-L337 (2005)

[9] T. Masuzawa, S. Kuniyoshi, M. Onishi, R. Kato, I. Saito, T. Yamada, A. T. T. Koh, D. H. C. Chua, T. Shimosawa, and K. Okano, "Conditions for a carrier multiplication in amorphous-selenium based photodetector," Appl. Phys. Lett. 102, 073506 (2013)

[10] K. Okano, I. Saito, T. Mine, Y. Suzuki, T. Yamada, N. Rupesinghe, G. A. J. Amaratunga, W. I. Milne and D. R. T. Zahn, "Characterizations of a-Se based photodetectors using X-ray photoelectron spectroscopy and Raman spectroscopy," J. Non-Cryst. Solids 353, 308-312 (2007)

[11] I. Saito, T. Masuzawa, Y. Kudo, S. Pittner, T. Yamada, A. T.T. Koh, D. H.C. Chua, Y. Mori, D. R.T. Zahn, G. A.J. Amaratunga and K. Okano, "Durability and photo-electric characteristics of a mille-feuille structured amorphous selenium (a-Se)–arsenic selenide (As2Se3) multi-layered thin film," Journal of Non-Crystalline Solids, 378, 96 (2013)

[12] K. Tanioka, J. Yamazaki, K. Shidara, K. Taketoshi, T. Kawamura, S. Ishioka and Y. Takasaki, "An Avalanche-Mode Amorphous Selenium Photo- conductive Layer for Use as a Camera Tube Target," IEEE Electron Device Lett. EDL-8, 9, 392-394 (1987)

[13] S. Kasap, J. A. Rowlands, S. D. Baranovskii and K. Tanioka, "Lucky drift impact ionization in amorphous semiconductors," J. Appl. Phys. 96 2037 (2004)

[14] A. Reznik, S. D. Baranovskii, O. Rubel, G. Juska, S. O. Kasap, Y. Ohkawa, K. Tanioka and J. A. Rowlands, "Avalanche multiplication phenomenon in amorphous semiconductors: Amorphous selenium versus hydrogenated amorphous silicon," J. Appl. Phys. 102, 053711 (2007)

[15] G. Pfister, "New aspects of electronic properties of amorphous selenium and its use in xerography," Contemp. Phys. 20, 449–479 (1979)

[16] S. Kasap, J.B. Frey, G. Belev, O. Tousignant, H. Mani, L. Laperriere, A. Reznik, J.A. Rowlands, "Amorphous selenium and its alloys from early xeroradiography to high resolution X-ray image detectors and ultrasensitive imaging tubes," Physica Status Solidi (b), 246, pp.1794-1805 (2009)

[17] M. W. Geis, J. C. Twichell, N. N. Efremow, K. Krohn, and T. M. Lyszczarz, "Comparison of electric field emission from nitrogen-doped, type Ib diamond, and boron-doped diamond," Appl. Phys. Lett. 68, pp.2294-2296 (1996)

[18] K Okano, T. Yamada, A. Sawabe, S. Koizumi, J. Itoh, and G. A. J. Amaratunga, "Metal-insulator- vacuum type electron emission from N-containing chemical vapor deposited diamond," Appl. Phys. Lett. 79, 275-277 (2001)

[19] O. Bubon, G. DeCrescenzo, W. Zhao, Y. Ohkawa, K. Miyakawa, T. Matsubara, K. Kikuchi, K. Tanioka, M. Kubota, J.A. Rowlands and A. Reznik, "Electroded avalanche amorphous selenium (a-Se) photosensor," Curr. Appl. Phys. 12 983 (2012)

[20] S. Abbaszadeh, N. Allec, S. Ghanbarzadeh, U. Shafique, K.S. Karim, "Investigation of Hole- Blocking Contacts for High-Conversion-Gain Amorphous Selenium Detectors for X-Ray Imaging," IEEE Trans. Electron Devices 59, no.9, pp.2403-2409 (2012)

[21] S. O. Kasap and J. A. Rowlands, "X-ray photoconductors and stabilized a-Se for direct conversion digital flat-panel X-ray image- detectors," J. Mater. Sci., Mater. Electron. 11, 179-198 (2000)

[22] H. Yamaguchi, T. Mine, Y. Suzuki, K. Okano, T. Yamada, and A. Sawabe, "Broad area electron emission from oxygen absorbed homoepitaxially grown nitrogen (N)-doped chemical vapor deposited diamond (111) surface," J. Vac. Sci. Technol. B 21, 1730 (2003)

Chapter 5. High-sensitivity photo detection in UV region

In this chapter, evaluation of quantum efficiency has been extended in the UV region, where it was found that the quantum efficiency of a-Se in UV range is up to two orders of magnitude greater than that in visible range. Field emission current *versus* applied voltage (I_{em}-V) characteristics of the detector are compared between under UV illumination and no illumination. The sensitivity of the photodetector is then evaluated in terms of external quantum efficiency, of which results are compared to solid-state UV detectors. The external quantum efficiency of a-Se based photodetector is up to two orders of magnitude higher than latest UV detectors. The present result may lead to ultra high-sensitivity UV photoelectric devices made of a-Se.

5.1. Advantages of a-Se based UV detector

Detection of weak ultraviolet (UV) light has attracted much attention in various fields, including astronomic observation, flame sensors for security use, transparent photovoltaic devices, as well as medical imaging [2-5]. A common UV detector is avalanche photodiode (APD) made from silicon, however, this device has high thermal noise due to a relatively narrow band gap. While using wide-gap semiconductors can reduce the thermal noise, APDs made from wide-gap semiconductors are not sensitive to visible light, and are not suitable for spectrometric applications.

a-Se is a promising material for a photodetector that can be applied to wide wavelength range covering visible, UV and X-ray [6-7]. In addition, a-Se based photodetector can exhibit extremely high sensitivity and wide dynamic range when combined into vacuum tube device. This high sensitivity mode is explained by signal

enhancement due to an internal carrier multiplication in a-Se, which leads to quantum efficiency of greater than 100% [8-10]. A high resistivity and wide optical band gap of a-Se (up to 2.0 eV) can reduce the dark current, which further enhance the sensitivity and dynamic range of the photodetector.

5.2. Fabrication and characterization of a-Se based UV detector

The prototype photodetector proposed in this study is essentially a single-pixel photo imaging device: this device is a diode-structured vacuum tube that consists of an a-Se based photoconductive anode and N-doped diamond electron emitter. Figure 5.2.1 shows a schematic diagram of the experimental setup.

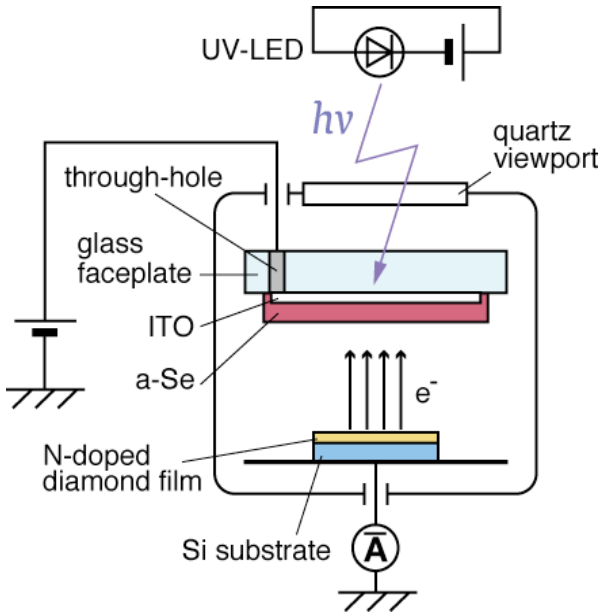

Figure 5.2.1. Schematic diagram of the photodetector, which consists of a-Se photoconductive anode and diamond electron emitter.

The anode is vacuum-evaporated a-Se film stabilized by As incorporation and low temperature annealing, whose substrate is glass faceplate equipped with electrical through-hole and ITO film serving as back contact. Optical absorption of the substrate and back contact is characterized by UV-visible spectroscopy. Figure 5.2.2 shows a typical

UV-visible spectrum of ITO thin film. The transmittance is calculated by taking a glass faceplate as reference, whose transmittance is more than 99.8 % of the air against the light with wavelength between 300 nm and 1100 nm. It is evident from UV-visible spectrum that absorption of ITO thin film becomes dominant at 350 nm or shorter wavelengths; therefore, UV light at around 350-400 nm is suitable for evaluating sensitivity of a-Se with current setup.

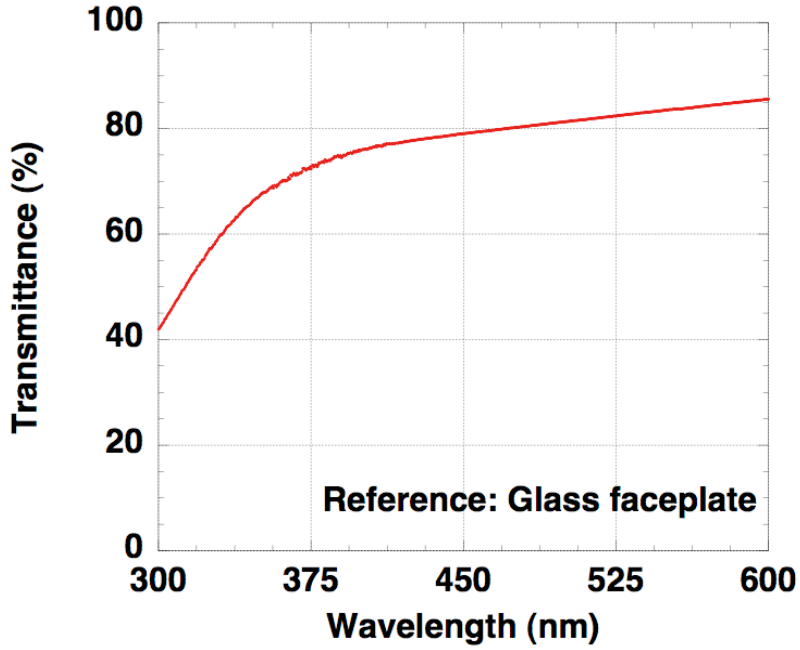

Figure 5.2.2. UV-visible spectrum of ITO thin film deposited as transparent contact. A glass faceplate is taken as reference.

Combined with a-Se anode, N-doped diamond thin film is mounted as a cathode for signal readout. The N-doped polycrystalline diamond is grown by CVD, using acetone as carbon source and urea as nitrogen source. Detailed fabrication process of N-doped diamond is presented in Chapter 4. A N-doped diamond having extraction voltage at around 400 V is selected as cathode, which is suitable for applying high voltage across the anode and the cathode to induce carrier multiplication in a-Se.

The a-Se anode and the diamond cathode are fixed in the measurement setup, whose structure is illustrated in Figure 5.2.1. The anode-cathode distance is kept at 100 μm using Teflon spacer. The setup is then introduced in a high vacuum chamber and evacuated to the pressure 4.0 x 10^{-8} Torr, where electron emission is induced by applying voltage between the anode and the cathode. The voltage is controlled by HP 4140B, whose output is multiplied by 1,000 times using Glassman high voltage DC power supply. The emission current is measured by Advantest R6441C digital multimeter with detection limit of 0.1 nA. An UV light-emitting diode with a typical wavelength of 375 nm (Nichia NSPU510CS) is fixed at a distance of 2 cm from the setup, and operated at 20 mA to illuminate the anode side of the photodetector through a quarts view port.

The operation mechanism of this device is explained as follows: the incident UV light generates electron-hole pairs in a-Se film, and some of the holes that accumulate in the anode surface are read-out as electrical signal by electron beam from diamond cold cathode. When the applied voltage is high enough to operate the device in high-sensitivity mode, the electric field across a-Se film is intense enough to initiate carrier multiplication, where photo-induced holes are multiplied in the a-Se, and emission current increases due to the increased hole accumulation.

Response to the UV light is confirmed by emission current *versus* applied voltage (I_{em}-V) characteristics of the detector. I_{em}-V characteristics are compared between with UV illumination and without illumination, which are illustrated as a-Se:UV and a-Se:Dark in Figure 5.2.3.

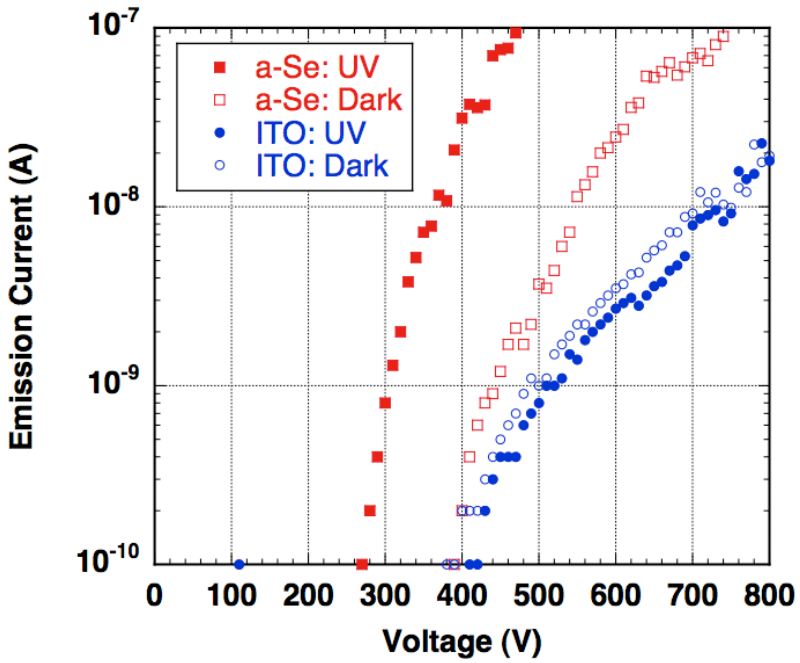

Figure 5.2.3. I_{em}-V characteristics of the prototype device with different anode (a-Se or ITO) and lighting conditions (UV ON or OFF).

The I_{em}-V curves show that the emission current at a fixed voltage (e.g. ~400 V) is up to two orders of magnitude larger under UV illumination than the dark current, proving a successful UV detection. The sensitivity of the photodetector is then evaluated in terms of quantum efficiency, which is the number of carriers generated per incident photon. Although this value involves various parameters such as generation recombination rate and carrier mobility, a simple estimation of *nominal quantum efficiency* is possible using the following equation:

$$\eta_{nom} = \frac{\Delta I}{eN_0(1-\exp(-\alpha D))} \qquad (5.2.1)$$

where e is the elemental charge, N_0 is a number of incident photon and ΔI is the photo current minus the dark current at a fixed voltage. The term $(1-\exp(-\alpha D))$ consists of the absorption coefficient α and the thickness of a-Se film, D: in order to simplify the discussion, here we assume that $(1-\exp(-\alpha D))$ as 1 to approximate the lower limit of the

nominal quantum efficiency. N_0 is calculated to be 1.4~2.0 x 10^{20} photons per square meters per second, using optical power output and directivity of the UV-LED supplied in the product datasheet. It is also assumed that the field-induced electron emission takes place in a local site on the cathode, of which area is reported to be 1 μm^2 or even smaller: Only the fraction of photons that illuminate this area should contribute to the current increase. The nominal quantum efficiency calculated in this way is as large as 1,000 at the applied voltage of 400 V, meaning that up to 10^3 carriers are generated per incident photon.

The calculated value suggests extremely high-sensitivity photo detection. Assuming that this single-pixel device is integrated to a photo imager, the sensitivity can be evaluated in terms of external quantum efficiency (EQE), which is commonly used to evaluate the sensitivity of oxide-based and organic UV detectors in the literature [2-4]. The EQE of a ZnO MSM photodetector is reported to be 177 %, and latest MISIM photodetector has EQE of 6,150 % [3]. The EQE estimated from the present result is 100,000 %, which is up to two orders of magnitude higher than that of conventional UV detectors. This clearly shows that the carrier multiplication in a-Se is a promising technology for high-sensitivity photo detection in visible to UV range.

It should be noted that no blocking layer is deposited on or beneath the a-Se film in this study: these blocking layers are reported to prevent carrier injection into a-Se film, which prevents dark current and enables one to apply high voltage across the film [8-10]. The carrier multiplication without blocking layers may be explained by diode-structured device using cold cathode: since the present device is driven by a cold cathode, emission current is negligibly small unless potential difference between the anode and the cathode is smaller than the extraction voltage of the cold cathode. Therefore, the blocking layer is

built in the insulating nature of cold cathode, which may enable carrier multiplication without blocking layers.

It should also be noted that the nominal quantum efficiency of a-Se based photodetector is reported to be 10 to 40 for visible light. A possible reason for the large difference in quantum efficiency between visible and UV light may be due to the number of photons estimated based on approximation. The number of incident photons in visible range was calculated assuming that all the incident photons have wavelength of 555 nm. However, this assumption could lead to underestimation of quantum efficiency: the halogen lamp used in the previous study had color temperature of 3,000 K, in which case most of the photons have wavelengths lower than 555 nm. The energy spectrum of the white light with color temperature 3,000 K is shown in Figure 5.2.4 [11]. Since a-Se has optical gap of 2.0 eV, photons with wavelength longer than 620 nm may not be captured in a-Se. As such, the actual number of incident photons that were captured in a-Se could be much smaller than the estimated amount, and the nominal quantum efficiency may be underestimated up to one order of magnitude.

Despite the above discussion, the difference in nominal quantum efficiency is too large to be explained by this underestimation. The present result may suggest that the carrier multiplication can depend on the wavelength of the incident light. A detailed comparison between response to visible and UV light, as well as further analysis on the carrier multiplication process, is currently ongoing.

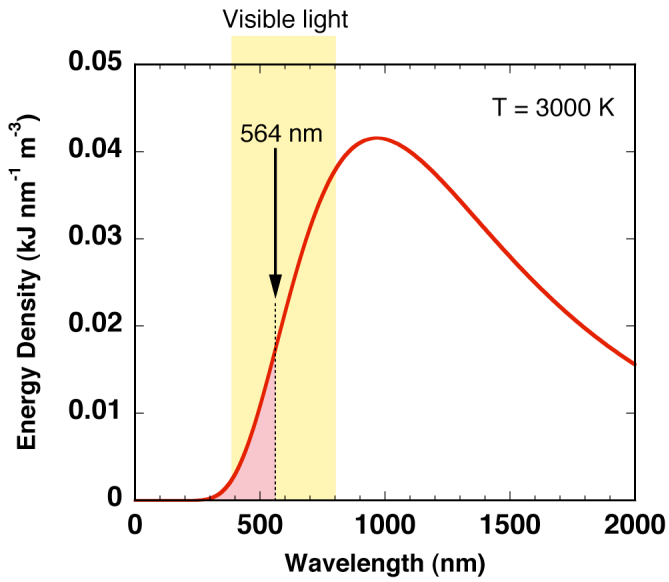

Figure 5.2.4. Radiation spectrum of a black body calculated based on Planck's law [11]

As a conclusion, a high-sensitivity UV detection has been demonstrated utilizing carrier multiplication in a-Se based photodetector. The sensitivity of the detector has been evaluated in terms of nominal quantum efficiency and EQE, of which result shows that the sensitivity of a-Se based photodetector is up to two orders of magnitude higher than conventional solid-state UV detectors. The result also indicates that the effect of carrier multiplication depends on the wavelength of incident light, which may lead to spectrometric photo detection. Such a high-sensitivity photodetector with wide detectable wave range is not only useful in practical applications, but is aspired in various photon-out analysis, for example, inverse photoemission spectroscopy, where energy of photons is essential for evaluating an electronic structure of a solid.

References

[1] T. Masuzawa, M. Onishi, I. Saito, T. Yamada, A. T. T. Koh, D. H. C. Chua, S. Ogawa, Y. Takakuwa, Y. Mori, T. Shimosawa, and K. Okano, "High quantum efficiency UV detection using a-Se based photodetector," Phys. Status Solidi RRL, 1–4 (2013) / DOI 10.1002/pssr.201307185

[2] C H. Lin and C W. Liu, "Metal-Insulator-Semiconductor Photodetectors," Sensors 2010, 10, 8797- 8826 (2010)

[3] J. Yu, C X. Shan, Q. Qiao, X H. Xie, S P. Wang, Z Z. Zhang, and D Z. Shen, "Enhanced Responsivity of Photodetectors Realized via Impact Ionization," Sensors 2012, 12, 1280-1287 (2012)

[4] X. Gong, M H. Tong, S H. Park, M. Liu, A. Jen and A. J. Heeger, "Semiconducting Polymer Photodetectors with Electron and Hole Blocking Layers: High Detectivity in the Near-Infrared," Sensors 2010, 10, 6488-6496 (2010)

[5] I. Saito, W. Miyazaki, M. Onishi, Y. Kudo, T. Masuzawa, T. Yamada, A.T.T. Koh, D.H.C. Chua, K. Soga, M. Overend, M. Aono, G.A.J. Amaratunga, and K. Okano, "A transparent ultraviolet triggered amorphous selenium p-n junction," Appl. Phys. Lett. 98, 152102 (2011)

[6] S. Abbaszadeh, K.S. Karim, and V. Karanassios, "Measurement of UV from a Microplasma by a Microfabricated Amorphous Selenium Detector," IEEE Trans. Electron. 60, 880-883 (2013)

[7] S. O. Kasap and J. A. Rowlands, "X-ray photoconductors and stabilized a-Se for direct conversion digital flat-panel X-ray image- detectors,"J. Mater. Sci., Mater. Electron. 11, 179-198 (2000)

[8] K. Tanioka, J. Yamazaki, K. Shidara, K. Taketoshi, T. Kawamura, S. Ishioka and Y. Takasaki, "An Avalanche-Mode Amorphous Selenium Photo- conductive Layer for Use as a Camera Tube Target," IEEE Electron Device Letters, EDL-8, 9, 392-394 (1987)

[9] S. Kasap, J. A. Rowlands, S. D. Baranovskii and K. Tanioka, "Lucky drift impact ionization in amorphous semiconductors," J. Appl. Phys. 96 2037 (2004)

[10] A. Reznik, S. D. Baranovskii, O. Rubel, G. Juska, S. O. Kasap, Y. Ohkawa, K. Tanioka and J. A. Rowlands, "Avalanche multiplication phenomenon in amorphous semiconductors: Amorphous selenium versus hydrogenated amorphous silicon," J. Appl. Phys. 102, 053711 (2007)

[11] C. Kittel, Introduction to Solid State Physics, 8 edition, Wiley (2004)

Chapter 6. Conclusion

As a conclusion, mechanism of high-sensitivity photo detection utilizing carrier multiplication in a-Se has been investigated. In the study, a-Se based prototype photodetector has been developed in order to evaluate its sensitivity in multiplication mode. Nitrogen-doped diamond was used to drive this device, aiming that the advantages of diamond cold cathode such as high stability and low-energy electron contribute to the device operation.

As a result, the carrier multiplication and high-sensitivity photo detection have been confirmed, and the nominal quantum efficiency of a-Se based photodetector was estimated to be 10 to 40 for visible light and as large as 1,000 for UV light. The wavelength-dependence of the carrier multiplication process should help further clarify the mechanism of carrier multiplication, which should lead to high-sensitivity imaging in the wavelength beyond visible and UV.

APPENDIX

Publication related to this study

Journal papers

1. T. Masuzawa, I. Saito, T. Yamada, M. Onishi, H. Yamaguchi, Y. Suzuki, K. Onuki, N. Kato, S. Ogawa, Y. Takakuwa, A. T.T. Koh, D. H.C. Chua, Y. Mori, T. Shimosawa, K. Okano, "Development of an Amorphous Selenium-Based Photodetector Driven by a Diamond Cold Cathode", *Sensors*, **13**, 13744 (2013) *Review article*

2. T. Masuzawa, M. Onishi, I. Saito, T. Yamada, A. T. T. Koh, D. H. C. Chua, S. Ogawa, Y. Takakuwa, Y. Mori, T. Shimosawa, K. Okano, "High quantum efficiency UV detection using a-Se based photodetector", physica status solidi - Rapid Research Letters, **7**, 473 (2013) *Selected as journal cover page*

3. T. Masuzawa, S. Kuniyoshi, M. Onishi, R. Kato, I. Saito, T. Yamada, A.T.T. Koh, D.H.C. Chua, T. Shimosawa, and K. Okano, "Conditions of high-sensitive photodetection in amorphous selenium based photodetector driven by diamond cold cathode", *Applied Physics Lett*ers **102**, pp.73506 (2013)

4. T. Masuzawa, Y. Sato, Y. Kudo, I. Saito, T. Yamada, A.T.T. Koh, A. D.H.C. Chua, T. Yoshino, W.J. Chun, S. Yamasaki, K. Okano, "Correlation between low threshold emission and C-N bond in nitrogen-doped diamond films", *Journal of Vacuum Science & Technology B* **29**, pp.02B119/1-02B119/6 (2011)

5. T. Masuzawa, Y. Shiraki, Y. Kudo, I. Saito, H. Yamaguchi, T. Yamada, and K. Okano, "Clarification of band structure at metal-diamond contact using device simulation", *Applied Surface Science* **254**, pp.6285-6288 (2008)

6. I. Saito, W. Miyazaki, M. Onishi, Y. Kudo, T. Masuzawa, T. Yamada, A. T. T. Koh, D. H. Chua, K. Soga, M. Overend, M. Aono, G.A.J. Amaratunga, and K. Okano, "A transparent ultraviolet triggered amorphous selenium p-n junction", *Applied Physics Letters* **98**, pp.152102 (2011)

7. Y. Kudo, Y. Sato, T. Masuzawa, T. Yamada, I. Saito, T. Yoshino, W.J. Chun, S. Yamasaki, K. Okano, "Field emission from N-doped diamond doped with dimethylurea", *Journal of Vacuum Science & Technology B* **28**, pp.506-510 (2010)

8. H. Yamaguchi, T. Masuzawa, S. Nozue, Y. Kudo, I. Saito, J. Koe, M. Kudo, T. Yamada, Y. Takakuwa and K. Okano, " Electron emission from conduction band of diamond with negative electron affinity", *Physical Review B* **80**, pp.165321-165325 (2009)

9. H. Yamaguchi, Y. Kudo, T. Masuzawa, M. Kudo, T. Yamada, Y. Takakuwa and K. Okano, "Combined x-ray photoelectron spectroscopy/ultraviolet photoelectron spectroscopy/field emission spectroscopy for characterization of electron-emission mechanism of diamond", *Journal of Vacuum Science & Technology B* **26**, pp.730-734 (2008)

10. H. Yamaguchi, T. Masuzawa, Y. Kudo, T. Yamada, M. Kudo, Y. Takakuwa and K. Okano, "Electron emission from natural type IIb diamond characterized by combined XPS/UPS/FES

system", *Diamond & Related Materials* **17**, pp.162-165 (2008)

11. Y. Kudo, T. Yamada, H. Yamaguchi, T. Masuzawa, I. Saito, S. Shikata, C. E. Nebel and K. Okano, "Field emission from modified P-doped diamond surfaced with different barrier height", *Japanese Journal of Applied Physics* **47**, pp.8921-8924 (2008)

Conference proceedings

12. 山田貴壽, 長谷川雅考, C. E. Nebel, 工藤唯義, 増澤智昭, 岡野健, 谷口尚, "n 型半導体立方晶窒化ホウ素単結晶からの電界放出機構", *信学技報* **111**, pp.47-52 (2011)
13. 山田貴壽, 長谷川雅考, C. E. Nebel, 工藤唯義, 山口尚登, 増澤智昭, 岡野健, "負の電子親和力を有する n 型半導体ダイヤモンドからの電界放出機構", *信学技報* **110**, pp.17-22 (2010)
14. 山田貴壽, 増澤智昭, 国吉真吾, 大西正徳, 齋藤市太郎, A.T.T. Koh, D.H.C. Chua, 下澤達雄, 岡野健, "ダイヤモンド冷陰極を用いたアモルファスセレン光検出器の特性評価", *第 26 回ダイヤモンドシンポジウム講演* , pp. 210-211 (2012)
15. 加藤理親, 岡野健, 久保謙哉, 増澤智昭, 山田貴壽, 友野大, 岡田信二, 上野一樹, 藤原裕也, 石田勝彦, 岩崎雅彦, "窒素添加ダイヤモンド中におけるミューオニウム生成測定", *第 26 回ダイヤモンドシンポジウム講演* , pp.214-215 (2012)
16. 増澤智昭, 国吉真吾, 大西正徳, 斎藤市太郎, Angel T.T. Koh, D.H.C. Chua, 山田貴壽, 下澤達 雄, 岡野 健, "アモルファスセレンとダイヤモンド冷陰極を用いた光検出器の評価", *信学技報* **112**, pp. 15-17 (2012)

Presentations in international conference

1. T. Masuzawa, S. Kuniyoshi, M. Onishi, I. Saito, A.T.T. Koh, D.H.C. Chua, T. Yamada, and K. Okano, "Carrier multiplication in a photodetector driven by diamond cold cathode", *International Vacuum Nanoelectronics Conference 2012,* Jeju, Korea (2012.7)
2. I. Saito, M. Onishi, K. Komiyama, W. Miyazaki, T. Masuzawa, Y. Kudo, A. Koh, D. Chua, K. Soga, M. Overend, M. Aono, G. A.J. Amaratunga, and K. Okano, "An amorphous selenium based UV sensitive photovoltaic device fabricated through electrolysis", *The Asia-Pacific Interdisciplinary Research Conference 2011,* Toyohashi, Japan (2011.11)
3. T. Yamada, M. Hasegawa, C. E. Nebel, Y. Kudo, T. Masuzawa and K. Okano, "Field Emission Mechanism of H-Terminated n-Type Diamond NEA Surface", *Material Research Society 2011 Fall Meeting*, Boston, U.S.A. (2011.11-12)
4. T. Masuzawa, Y, Kudo, Y. Sato, I. Saito, T. Yamada, A. T. T. Koh, D. H. C. Chua, T. Yoshino, W. J. Chun, S. Yamasaki and K. Okano, "Field Emission Mechanism of Nitrogen-doped Diamond with Different C-N Concentration", *Material Research Society 2011 Spring Meeting,* San Francisco, U.S.A. (2011.4)
5. T. Yamada, M. Hasegawa, Y. Kudo, M. Masuzawa, C. E. Nebel, K. Okano and T. Taniguchi, "Field emission properties from n-type semiconductors with NEA", *Japan Korea Vacuum Nanoelecronics Symposium,* Seoul, Korea (2011.)
6. I. Saito, W. Miyazaki, M. Oonishi, Y. Kudo, T. Masuzawa, T. Yamada, A. Koh, D. Chua, K. Soga, M. Overend, M. Aono, G. Amaratunga and K. Okano, "Transparent UV Solar Cells Utilizing Simply Fabricated Amophous Selenium p-n Junction", *Material Research Society 2011 Spring Meeting*, San Francisco, U.S.A. (2011.4)
7. T. Masuzawa, R. Kato, M. Onishi, Y. Kudo, I. Saito, T. Yamada and K. Okano, "Ultraviolet Photodetector Driven by Diamond Cold Cathode", *Material Research Society 2011 Fall Meeting,* Boston, U.S.A. (2011.11-12)
8. T. Masuzawa, R. Kato, M. Onishi, Y. Kudo, I. Saito, T. Yamada and K. Okano, "Ultraviolet Photodetector Driven by Diamond Cold Cathode", *The Asia-Pacific Interdisciplinary Research Conference 2011*, Toyohashi, Japan (2011.11)
9. T. Masuzawa, M. Onishi, R. Kato, W. Miyazaki, I. Takahashi, K. Okano, "Ultraviolet photodetector using a-Se anode and diamond cold cathode", *International Vacuum Nanoelectronics Conference 2011*, Vuppertal, Germany (2011.7)
10. T. Masuzawa, S. Kuniyoshi, M. Onishi, R. Kato, I. Saito, T. Yamada, A. T. T. Koh, D. H. C. Chua, T. Shimosawa, and K. Okano, "Amorphous selenium-based high sensitivity photodetector driven by diamond cold cathode", *The Irago Conference,* Toyohashi (2012.)
11. I. Saito, M. Onishi, I. Takahashi, T. Masuzawa, T. Yamada, A.T.T. Koh, D.H.C. Chua, M. Overend, K. Soga, Y. Mori, K. Okano, "Aerosol deposition of selenium thin films for energy generating smart glass", *The Irago Conference*, Toyohashi (2012.)